ACS OMEGA

Article

http://pubs.acs.org/journal/acsodf

Design, Synthesis and Evaluation of Bifunctional Acridinine−Naphthalenediimide Redox-Active Conjugates as Antimalarials

Srikanta Dana,[†,§] Sudhir Kumar Keshri,[†] Jyoti Shukla,[†] Kunwar Somesh Vikramdeo,[‡] Neelima Mondal,[‡] Pritam Mukhopadhyay,*[,†] and Suman Kumar Dhar*[,§]

[†]Supramolecular and Material Chemistry Lab, School of Physical Sciences, Jawaharlal Nehru University, New Mehrauli Road, 110067 New Delhi, India

[‡]School of Life Sciences, Jawaharlal Nehru University, New Mehrauli Road, 110067 New Delhi, India

[§]Special Centre for Molecular Medicine, Jawaharlal Nehru University, New Mehrauli Road, 110067 New Delhi, India

Supporting Information

ABSTRACT: A novel class of bifunctional molecules was synthesized integrating acridine (Ac) and redox-active naphthalenediimide (NDI) scaffolds directly and through a flexible linker (en). We evaluated in vitro antiplasmodial activity, physicochemical properties, and a possible mode of action. Theoretical studies suggested electronic segmentation between the electron-rich Ac and electron-deficient NDI scaffolds. Orthogonal Ac−NDI molecules showed activities in the micromolar to submicromolar range against a chloroquine (CQ)-sensitive strain of human malaria pathogen *Plasmodium falciparum* (maximum activity, IC_{50}: 0.419 μM). The flexible Ac−en−NDI molecules were most potent and showed activity in the nanomolar range against both CQ-sensitive (with most effective compounds, IC_{50}: 3.65 and 4.33 nM) as well as CQ-resistant (with most effective compounds, IC_{50}: 52.20 and 28.53 nM) strains of *P. falciparum*. Significantly, with CQ-resistant strains, the activity of the most effective compounds was 1 order of magnitude better than that of standard drug CQ. Ac−en−NDI-conjugated molecules were significantly more potent than the individual NDI and Ac-based molecules. The structure−activity relationship (SAR) suggests that the flexible spacer (en) linking the Ac and NDI scaffolds plays a vital role in exhibiting improved potency. None of the molecules triggered hemolysis in culture, and the most potent compounds did not show cytotoxicity in vitro against mammalian fibroblast NIH3T3 cells at their respective IC_{50} values. The other significant outcome of this work is that some of the investigated molecules have the potential to affect multiple processes in the parasite including the hemozoin formation in digestive vacuoles (DVs), mitochondrial membrane potential, and the redox homeostasis of the parasite.

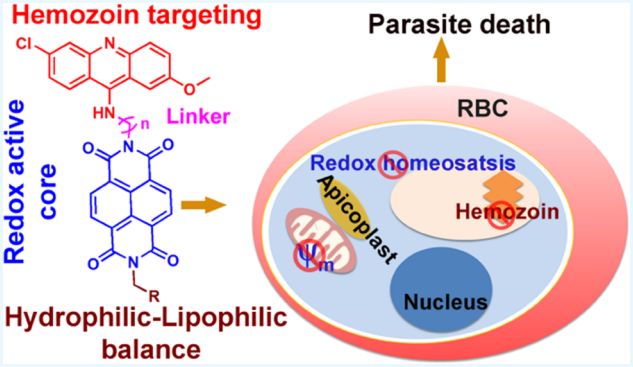

INTRODUCTION

Malaria, caused by an apicomplexan parasite of the genus *Plasmodium*, remains one of the world's greatest health challenges along with tuberculosis and AIDS. According to World Health Organization's (WHO) 2014 world malaria report, globally 198 million cases of malaria were reported in 2013, which have accounted for the loss of 584 000 human lives.[1] Chemotherapy has long been the mainstay for the control and eradication of malaria as no effective vaccine against malaria is available in the market.[2,3] Resistance to currently available antimalarial drugs, including artemisinin and artemisinin-based combination therapy (ACT), has become a major threat in malaria chemotherapy.[4,5] Combination therapy, where two or more drugs with different biological functions are coformulated in a single tablet, has limitations of high cost and risk of unwanted drug−drug interactions.[6] Therefore, it is very important to search for new chemotherapeutic strategies to develop effective and affordable new antimalarial drugs.

The concept of fusing two different pharmacophores with individual intrinsic activity to produce a single bifunctional agent known as hybrid drug designing has recently attracted immense interest of the medicinal chemistry community owing to the capability of bifunctional drugs to overcome drug resistance.[7−9] Indeed, a number of bifunctional drugs have been successfully applied in the treatment of cancer,[10] bacterial infection,[11] fungal infection,[12] and several pathogenic diseases including malaria,[7−9] leishmaniasis,[13] and trypanosomiasis.[14] The integration of individual pharmacophores leads to a new molecular electronic profile quite different from that of

Received: May 28, 2016
Accepted: June 30, 2016
Published: September 1, 2016

DOI: 10.1021/acsomega.6b00060
ACS Omega 2016, 1, 318−333

individual pharmacophores in the bifunctional molecule. This change in the molecular electronic profile could be modulated to manifest effectiveness in the bifunctional molecules against drug-resistant strains. Importantly, in the bifunctional molecule, two pharmacophores act on different targets with their independent mode of action that makes the emergence of drug resistance less likely.[7−9] Several problems with the known pharmacophores, for example, poor solubility, low bioavailability due to short retention time in bloodstream, and poor cell permeability, can be resolved by judicious designing of bifunctional molecules.[10] There can be several benefits of the bifunctional molecular approach, which includes (a) tailorability in synthesis, (b) potentially lower cost of synthesis, and (c) lower risk of adverse drug−drug interactions compared to the multicomponent drugs in a single tablet.[6−9] In this context, it is important to note that bifunctional molecules such as trioxaquine (PA1103/SA4R116242)[15] and ferroquine (Fq/SSR97193)[16] are under clinical trials as hybrid antimalarial agents.

The acridine (Ac)-based compounds are well known for their wide range of biological activities such as antimicrobial,[17] antitumoral,[18] antiprion,[19] anti-Alzheimer,[20] antileishmanial, antitrypanosomal,[21] and antimalarial activities.[22] Quinacrine (QN), a 9-amino Ac, has been used for the treatment of malaria with limited success.[23] Recently, we have successfully evaluated the antimalarial activity of acriflavine, an Ac-based dye, and its mechanism of action (MOA).[24]

In recent times, the redox homeostasis of malarial parasites has emerged as a valid drug target in malaria chemotherapy.[25] The parasite is exposed to high fluxes of reactive oxygen species (ROS) released from heme and decomposition products generated in the course of the major hemoglobin digestion process during its intraerythrocytic life cycle. An effective thiol-based redox network is present in *Plasmodium* to protect it from high fluxes of ROS. Thus, maintaining intracellular redox equilibrium is very important for the survival of the parasite.[26] Recent studies have revealed that redox-active agents, such as derivatives of 1,4-naphthaquinone, are able to disrupt the intracellular redox balance of the parasite, which results in the death of the parasite.[25,27] Further, the parasite mitochondrial electron transport chain (mETC) is involved in certain redox reactions (electron transfer process) of metabolic importance. Atovaquone, a redox-active drug, is known to interfere with the electron transfer process in the mETC, which results in the loss of the mitochondrial membrane potential.[28,29] Systematic studies on this type of redox-active molecule acting as an antimalarial drug have been extremely scarce. In this context, we wanted to explore the therapeutic potential of bifunctional molecules having redox-active scaffolds conjugated with known antimalarials.

Naphthalenediimides (NDIs) because of their novel properties, for example, optoelectronic, self-assembly, n-type semiconductor, anion recognition and transport, DNA binding, and antitumor properties, have gained phenomenal interest.[30−43] The unique structure of NDI, where four carbonyl groups lie coplanar to an extended aromatic ring system, allows interactions between the guanine amino group of DNA base pairs and the intercalated ring systems (via O atom of imide), making them an efficient DNA binding motif. The DNA binding property of NDI has led to the discovery of various NDI-based molecules exhibiting anticancer activity.[41−43] Tetra-substituted NDI derivatives have been reported to bind G quadruplexes and exert in vivo antitumor activity.[44,45] Substituents on NDI greatly affect the DNA binding mode and affinity.[46] Amino-acid-functionalized arylene diimide derivatives are of special interest as biomimetic advanced functional materials for wide spread application in fields ranging from biomedicine to electronics.[47] Peptide-functionalized NDI compounds containing more than one unit of NDI are known for threading polyintercalation to DNA, and the long-lived DNA-bound complex suggested great therapeutic potential of these compounds by altering the regulation of gene expression in cells.[48,49] Importantly, an NDI moiety has been extensively used to synthesize several redox-active functional molecules, where the NDI moiety undergoes one-electron reduction to generate an NDI radical anion ($NDI^{\bullet-}$).[50,51] We have demonstrated selective electron transfer (SET) from various analytes to generate persistent $NDI^{\bullet-}$ under ambient conditions.[52,53] Recently, we also isolated ambient stable NDI radical ions.[54] In addition, pioneering research has been carried out with $NDI^{\bullet-}$ for the fabrication of organic conductors, NIR absorptive nanotubes, chiral gels, and so forth.[55−57]

In the search for the new antimalarial drugs with new targets, essential biological redox processes happening inside of the parasite, for example, redox homeostasis in the cytoplasm and[25−27] electron transfer processes in mitochondria (mETC),[28,29] are fascinating targets. The redox activity of NDI suggests that it can be a promising scaffold along with known antimalarial agents to enhance its activity. To the best of our knowledge, an NDI scaffold has not been integrated with known antimalarial pharmacophores to develop bifunctional therapeutics to date. Herein, we report the design and synthesis of different classes of conceptually new Ac−NDI bifunctional molecules. The new classes of Ac−NDI molecules constitute (a) directly linked Ac with NDI (Ac−NDI), molecules **1a−e**, (b) Ac linked with NDI through a flexible spacer (Ac−en−NDI, en = spacer), molecules **2a−c**, (c) a salt of antioxidant citrate **3**, and (d) individual pharmacophore units, molecules **4** and **5**. We evaluated the in vitro antimalarial activity, theoretical physicochemical properties, and antimalarial MOA of these molecules. This provided us with a set of diverse class of bifunctional molecules with interesting electronic, redox, and H-bonding properties. The molecular design allowed us to tune the polarity of the molecules by altering the axial groups in the NDI scaffold. In addition, the linkage between the Ac and NDI scaffolds could be modulated in a flexible (**2a−c**) or rigid manner (**1a−e**). Further, a bifunctional molecular designing approach enables access to multiple cellular processes such as hemozoin, redox homeostasis, and mitochondrial membrane potential of the parasite by a single agent. This was reflected in the better antimalarial activity of hybrids **2a** and **2b** compared to that of standard antimalarial drug chloroquine (CQ) against both CQ-sensitive and CQ-resistant strains. The IC_{50} values of hybrids **2a** and **2b** were found to be better than those of the individual pharmacophores **4** and **5**.

RESULTS AND DISCUSSION

Design and Synthesis. We hypothesized that the NDI scaffold might facilitate the antimalarial activity of bifunctional molecules by virtue of its (a) ability to interact with DNA by its planar π-extended aromatic rings, (b) H bond formation ability of the O atoms of the four imide groups with biological targets, and (c) redox activity, that is, its ability to undergo one-electron reduction to form $NDI^{\bullet-}$ that may perturb the redox homeostasis of the parasite by interfering with the essential electron transfer processes happening in the cytoplasm and/or

DOI: 10.1021/acsomega.6b00060
ACS Omega 2016, 1, 318−333

Scheme 1. Molecular Structures of Ac−NDI Hybrid Molecules[a]

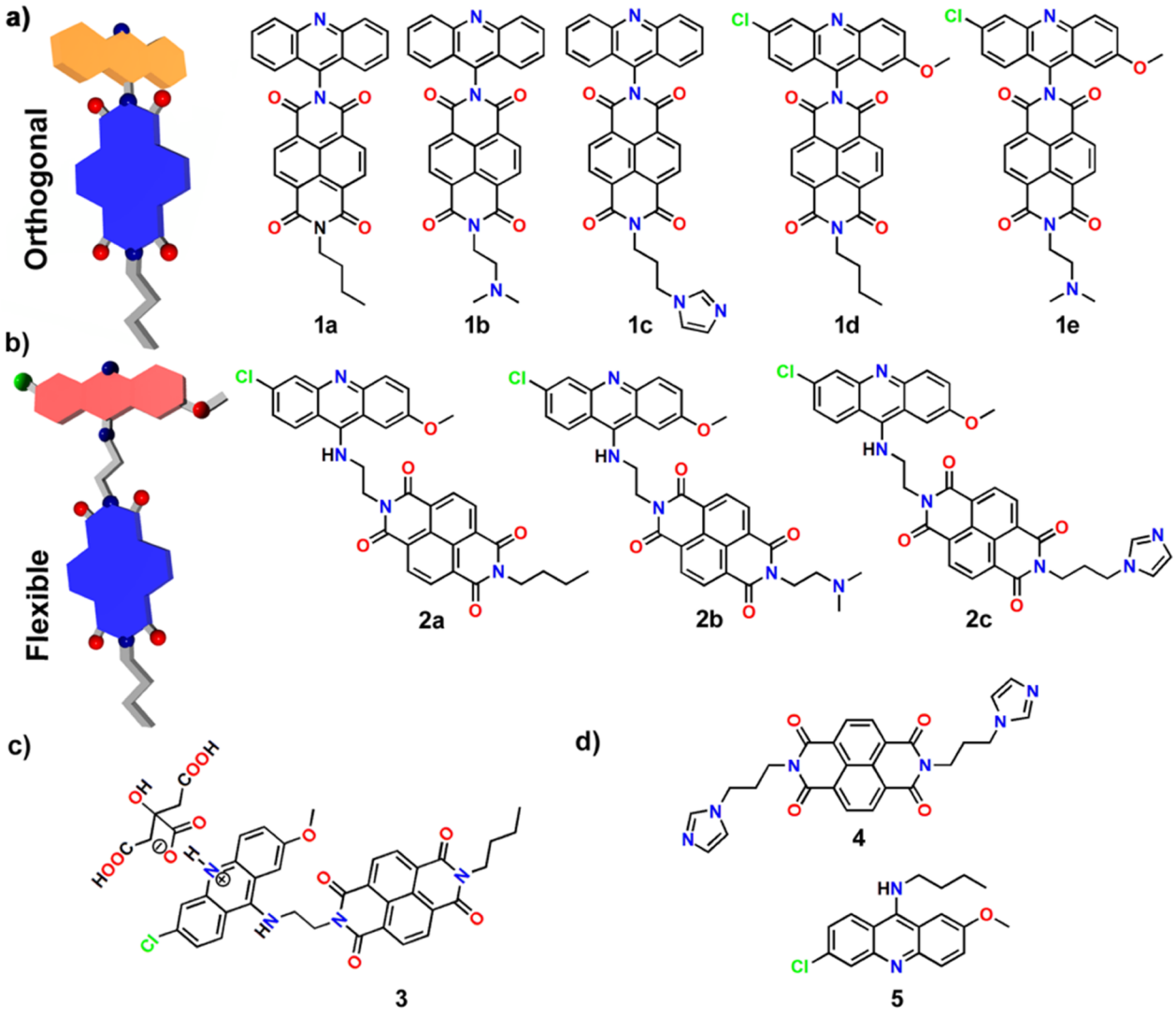

[a](a) Orthogonal design and corresponding orthogonal Ac−NDI hybrid molecules (**1a−e**), (b) flexible design and corresponding Ac−en−NDI hybrid molecules (**2a−c**), (c) citrate salt (**3**), and (d) NDI (**4**) and 9-amino Ac (**5**).

the mitochondria. On the other hand, the conjugation of Ac with NDI through a covalent linker would produce a bifunctional molecule, which is electronically segmented, that is, having both electron-rich and electron-deficient scaffolds integrated within the same molecule. This novel electronic profile may confer better characteristics in terms of hydrophilic−lipophilic balance (HLB), activity, and effectiveness against drug-resistant strains, which can be beyond the scope of the individual scaffolds. On the basis of these attributes, we integrated the Ac scaffold with the NDI to obtain a diverse range of Ac−NDI molecules (Scheme 1). In our design, the modulation of HLB of the Ac−NDIs can also be achieved upon varying the alkyl segments, which are linked axially to the NDI scaffold. The ESP of **2a** unequivocally established our prediction of an electronically segmented molecule (Figure 1). The differential ESP of the Ac and the NDI scaffolds in **2a** compared to that of the NDI scaffold in **NDI(C$_4$)** and the Ac scaffold in **5** is clearly evident from Figure 1. Further, the electronic segmentation of **2a** was confirmed from the highest occupied molecular orbital (HOMO) and lowest unoccupied molecular orbital (LUMO) surfaces. The HOMO and the

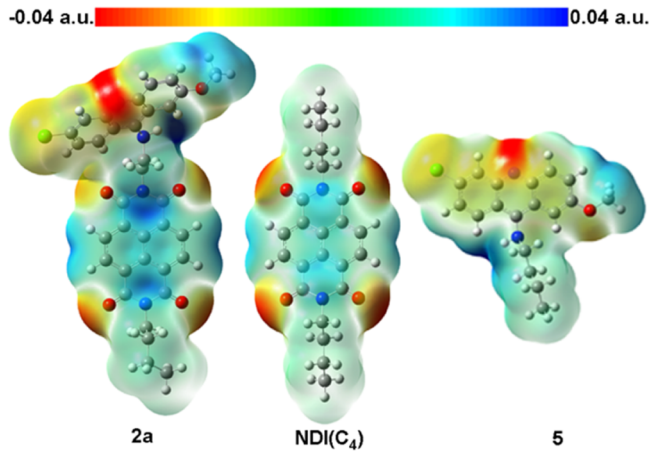

Figure 1. Electrostatic surface potential (ESP) of **2a**, **NDI(C$_4$)**, and **5** showing differential ESPs of Ac and NDI scaffolds in **2a** in comparison those of to the NDI scaffold in **NDI(C$_4$)** and Ac scaffold in **5**.

DOI: 10.1021/acsomega.6b00060
ACS Omega 2016, 1, 318−333

Scheme 2. Synthesis of (a) Orthogonal Ac-NDI (1a−e) and (b) Flexible Ac−en−NDI Molecules (2a−c) and Citrate Salt (3)

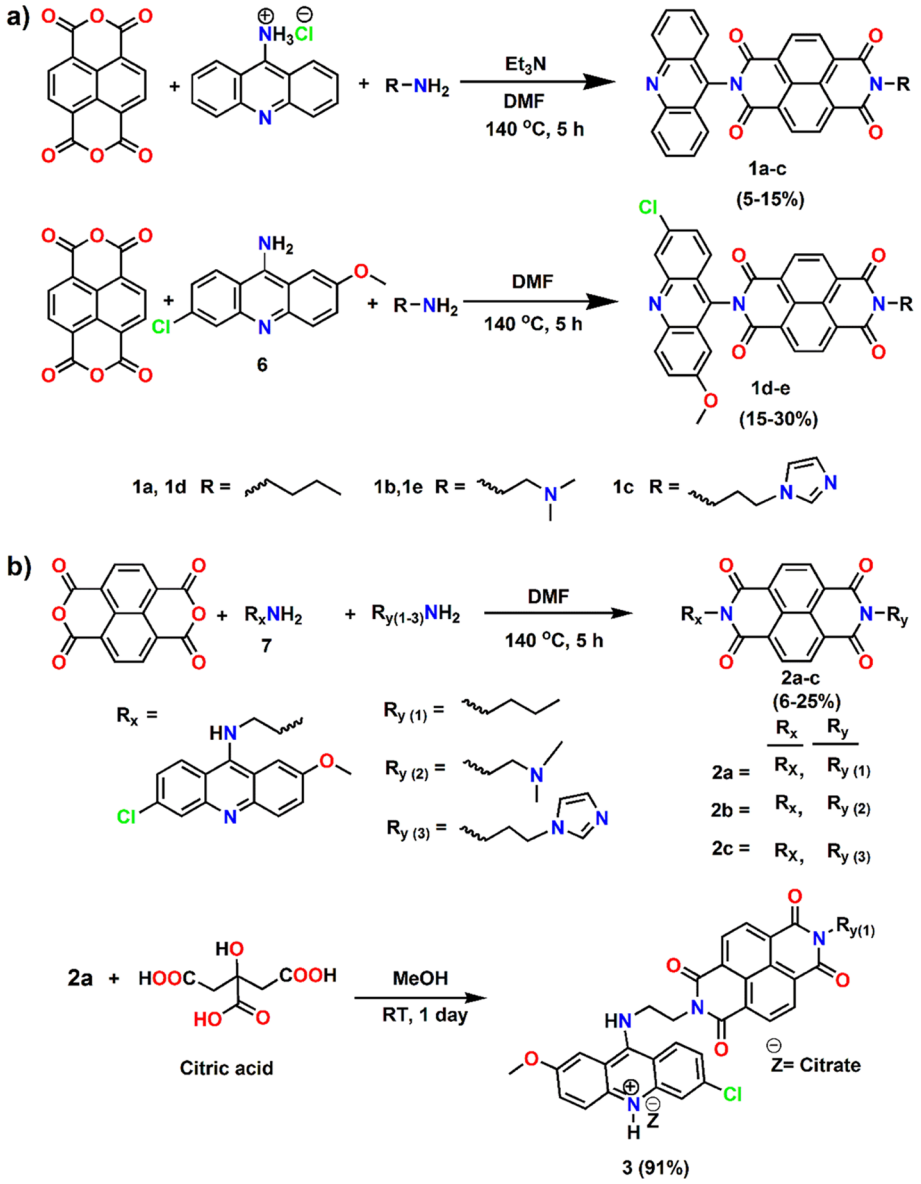

LUMO surfaces were found to be localized on the electron-rich Ac and the electron-deficient NDI scaffolds, respectively (Figure S1).

Toward the various bifunctional molecules, we designed and synthesized three classes of NDI-based molecular systems: (a) orthogonal Ac−NDI (**1a−e**), (b) flexible Ac−en−NDI (**2a−c**), and (c) an ion pair **3** containing the antioxidant citrate moiety. Apart from these three classes, we also synthesized the individual molecules **4** and **5** (Scheme 1). The orthogonal Ac−NDIs and flexible Ac−en−NDIs were synthesized in a straightforward manner using a one-pot synthetic approach that entails a condensation reaction of the naphthalenetetracarboxylicacid dianhydride (NTCDA) unit with appropriate derivatives of the 9-amino Ac (R_x) and the alkyl amine (R_y), as outlined in Scheme 2a,b. Appropriate 9-amino Acs (**5**, **7**) (Scheme 3) were synthesized via the aromatic nucleophilic substitution of 6,9-dichloro-2-methoxy Ac with an excess of alkyl amine or diamino ethane under an inert atmosphere.[58,59] The treatment of 6,9-dichloro-2-methoxy Ac with ammonium carbonate in phenol furnished the 9-amino-6-chloro-2-methoxy

Scheme 3. Synthesis of 9-Amino Ac (5) and Ac Amines (6−7)

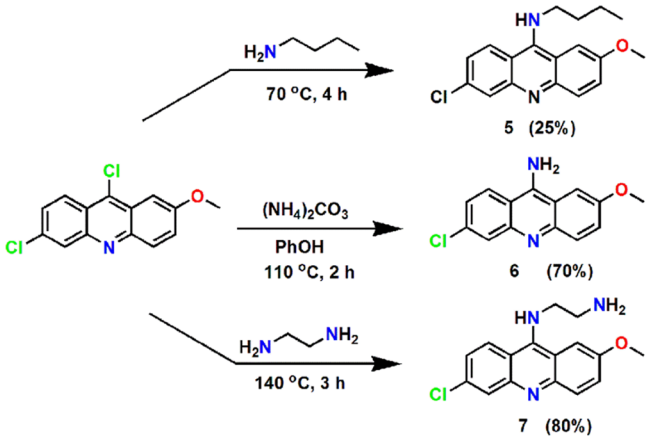

DOI: 10.1021/acsomega.6b00060
ACS Omega 2016, 1, 318−333

Ac (**6**) (Scheme 3).[60] The 9-amino Acs (**6**–**7**) were purified by precipitation in water medium with 70–80% isolated yields and were pure enough to be engaged for the synthesis of the next step. The NDI-based bifunctional molecules were synthesized by a condensation reaction of NTCDA with appropriate Ac amine and alkyl amine in *N*,*N*-dimethylformamide (DMF) and purified by column chromatographic separation affording 5–30% yield. Citrate salt **3** was prepared in excellent yield from the reaction of **2a** with citric acid in methanol. The characterization of these molecules was carried out by NMR, FTIR, and MALDI-TOF mass spectrometry (Supporting Information). A detailed account of the synthesis and characterization has been given in the experimental procedures.

The single crystal X-ray structure of **1b** revealed an orthogonal orientation of the two π surfaces (Ac and NDI) (Figure 2, Table S1, and Experimental Section). It is also clearly

Figure 2. Single crystal structure of compound **1b**, showing that Ac and NDI scaffolds are orthogonal to each other.

evident from the crystal structure of **1b** that each of the pharmacophores (Ac and NDI) is capable of generating multiple noncovalent interactions (NDI: π–π interaction and H bonding, Ac: H bonding) to form the self-assembled crystal lattice (Figure S2).

Antiplasmodial Activity and Structure–Activity Relationships (SARs). The in vitro antimalarial activity of a compound is evaluated by the amount of compound required to inhibit 50% of the growth of various *Plasmodium falciparum* strains (IC_{50}). All (11 new derivatives) of the Ac–NDIs and other molecules synthesized as described above (Scheme 1) were subjected to screening for in vitro antimalarial potency against *Pf* 3D7 (CQ-sensitive *P. falciparum* strain) using a microtiter-based SYBR Green I fluorescence assay.[61] All of the experiments were carried out twice and with duplicate samples. Data are reported as the geometric mean of IC_{50} values ±SD (standard deviation) obtained from two individual experiments (Table 1). The growth inhibition curves of all of the molecules are presented in the Supporting Information.

Amongst the 11 molecules tested, five molecules (**2a–c**, **3**, and **5**) exhibited good potency (IC_{50} < 100 nM) against the CQ-sensitive 3D7 strain. The remaining compounds had IC_{50} values ranging between 260 and 4197 nM as described in Table 1. Orthogonal Ac–NDIs (series a: **1a–e**; >0.4–4.0 μM) demonstrated considerably less antiplasmodial activity than the flexible Ac–en–NDIs (series b: **2a–c**; <10 nM).

SAR studies indicate that the incorporation of the 6-chloro-2-methoxy-substituted Ac scaffold into **1a–b** has a significant

Table 1. In Vitro Antimalarial Activity of Compounds 1–5 against *P. falciparum* (CQ-Sensitive) 3D7 and (CQ-Resistant) W2 Strains

	IC_{50} (nM)[a]				
entry	*Pf* 3D7	*Pf* W2	RI[b]	CC_{50} (nM)[c]	SI[d]
1a	4197 ± 206	nd[e]		nd	
1b	545 ± 165	nd		nd	
1c	780 ± 129	nd		nd	
1d	3778 ± 231	nd		nd	
1e	419 ± 16.16	nd		nd	
2a	3.65 ± 1.03	52.20 ± 0.34	14.30	>20	>5.48
2b	4.33 ± 0.76	28.53 ± 5.33	6.58	>20	>4.62
2c	8.44 ± 1.18	nd		nd	
3	3.89 ± 0.81	nd		nd	
4	260.20 ± 6.01	nd		nd	
5	26.40 ± 13.54	nd		>20	>0.75
CQ[f]	12.56 ± 0.66	430.60 ± 1.05	34.28	nd	

[a]IC_{50} values are the mean of two independent experiments (each experiment was carried out with duplicate samples) for each strain ± standard deviation. [b]Resistance index (RI) = IC_{50} (W2)/IC_{50} (3D7). [c]CC_{50} (50% cytotoxic concentration) was determined in mammalian fibroblast NIH3T3 cells. [d]Selectivity index (SI) = CC_{50}/IC_{50} (3D7). [e]nd = not determined. [f]CQ = chloroquine.

positive effect on the antiplasmodial activity. Thus, the IC_{50} values for **1a–b** reduced from 4197 and 545 nM to 3778 and 419 nM, respectively, for **1d–e**. On the basis of the considerable evidence that quinoline- and Ac-based antimalarials inhibit hemozoin formation by forming complexes between the heme and compound through π–π stacking interactions between the aromatic ring of the compound and the porphyrin ring system,[58,62–67] it can be assumed that the introduction of these two substituents enhances the stability of complexation with heme. The introduction of basic nitrogen ($-NMe_2$, imidazole) into the alkyl chain (R_y) of **1b–c** and **1e** (IC_{50} values 545, 780, and 419 nM, respectively) greatly improved the antimalarial activity on the CQ-sensitive strain in comparison to the less basic alkyl chain bearing **1a** and **1d** (4197 and 3778 nM, respectively). The beneficial effect of basic nitrogen in the alkyl chain can be attributed to the enhanced accumulation of **1b–c** and **1e** in the digestive vacuole (DV) of the parasite. This also supports the notion that the basicity of the alkyl chain in these molecules plays a crucial role similar to known quinoline- and Ac-based antimalarials.[64–71] The spacer linking Ac and NDI had a dramatic influence on the antimalarial activity. Flexible Ac–en–NDI (series b) with an amino-alkyl spacer exhibited higher activity than orthogonal Ac–NDIs (series a) without a spacer against the 3D7 strain. **2a** and **2b** (3.65 and 4.33 nM) were nearly 1000- and 100-fold more active against 3D7 than the **1d** and **1e**, respectively. The higher activity of **2a–b** may be attributed to mode of binding of these compounds to the heme. On the basis of the available binding model of the quinoline ring with hematin,[72–74] it can be proposed that the presence of the –NH group in the spacer of the Ac–en–NDI hybrids enhances the stability of the heme–compound complex by forming a H-bond between the –NH group and –COOH group of the hematin. In the proposed model (Figure S3a), imide oxygen of the NDI also serves as a multiple H-bond acceptor unit and can also form a H-bond with the –COOH group of the hematin, thus providing extra stability to the complex. We anticipate that

DOI: 10.1021/acsomega.6b00060
ACS Omega 2016, 1, 318–333

the rigid structure of orthogonal Ac−NDIs did not allow the NDI scaffold to form effective H-bonds with the −COOH group of hematin. In the class of flexible molecules (**2a−c**), the increase in basicity of the alkyl chain did not play a dominant role in their activity, whereas in the case of orthogonal Ac−NDI series, basicity had played a predominant role. Compound **3** (citrate salt of **2a**) and **2a** also displayed a nearly similar activity (3.89 and 3.65 nM, respectively). Compounds **2a−c** and **3** exhibited more potency, for example, 3.4-, 2.9-, 1.5-, and 3.2-fold, respectively, compared to CQ against the 3D7 strain.

Finally, the most potent molecules **2a−b** from the flexible Ac−en−NDI series were screened for their potency against *Pf* W2 (CQ-resistant *P. falciparum* strain) using microtiter-based SYBR Green I fluorescence assay. **2a−b** (52.20, 28.53 nM) exhibited ∼8- and 15-fold higher antimalarial activity, respectively, than CQ (430.60 nM) against the *Pf* W2 strain, and they also displayed comparatively better RIs than CQ (Table 1). **2b** was nearly 2-fold more active than **2a** against the CQ-resistant strain. This higher activity of **2b** against the resistant strain can be attributed to the intramolecular H-bond formation ability of **2b** at physiological pH. Guy et al. demonstrated that the incorporation of the intramolecular H-bonding motif in the side chain enhances the antimalarial potency of compounds against the CQ-resistant W2 strain.[75] In our case, **2b** contains a H-bond acceptor ($-NMe_2$) on the alkyl chain, which will be protonated at physiological pH that allows the intramolecular H-bonding between the protonated terminal amine (H-bond donor) and the oxygen atom of the imide group in NDI (Figure S3b). This type of intramolecular H-bond formation is not possible in **2a** because of the lack of the $-NMe_2$ functional group.

To ascertain specific benefits of the Ac-NDI conjugate over the individual constituents, the respective individual NDI (**4**) and Ac (9-(*N*-butyl) amino-6-chloro-2-methoxy-Ac (**5**)) were screened for antimalarial activity (Figure 3). Notably, both the

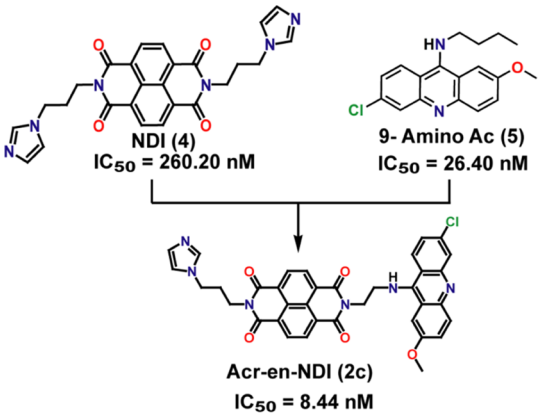

Figure 3. Antimalarial activity of Ac−en−NDI (**2c**) compared to individual components NDI (**4**) and 9-amino Ac (**5**).

individual NDI (**4**, IC_{50} = 260 nM) and Ac (**5**, IC_{50} = 26.4 nM) displayed significantly decreased potency over Ac−en−NDI (**2c**, IC_{50} = 8.44 nM) against *P. falciparum*, thereby demonstrating the potency of the NDI scaffold in the conjugated Ac−NDI pharmacophore. It is important to recall that the effect of an increase in the basicity of Ac−en−NDIs does not reflect in their antimalarial activity, and also their antimalarial activity is quite high (<10 nM). This may be attributed to the existence of other drug targets of Ac−en−NDIs outside of the DV, in addition to the hemozoin formation. Thus, the NDI scaffold in these Ac−NDIs may be able to act on other drug targets and play a significant role in the higher activity of these conjugate molecules. It is pertinent to mention that the Ac−NDIs represent a more promising scaffold over individual Ac/NDI because the probability of the emergence of resistance against a hybrid pharmacophore is always likely to be less than that in the case with individual pharmacophores.

Assessment of the Cytotoxicity of the Most Potent Molecules. The cytotoxicity (CC_{50} values, Table 1) of the most potent molecules **2a−b** was determined against mammalian (fibroblast NIH3T3) cells using final concentrations ranging from 0.625 to 20 nM by MTT assay. No relevant CC_{50} could be obtained in the concentration range tested. On the basis of these data, we extrapolated a CC_{50} value >20 nM for all tested compounds (Figure S4). The studies reveal that the **2a−b** are not significantly cytotoxic at their corresponding antimalarial IC_{50} values. Further, we also evaluated the SIs [SI = {CC_{50} (NIH3T3)}/{IC_{50} (*Pf* 3D7}] of all of these compounds (Table 1). **2a−b** exhibited moderate SI values (>5.5 and >4.6). It is to be noted that even at higher micromolar drug concentrations tested for the antimalarial activity (20−40 μM), the absence of hemolysis of the infected and the noninfected red blood cells (RBCs) may ascertain that these molecules may produce minimum adverse effects in blood circulation even at higher concentrations.

Physicochemical Properties of the Conjugate Molecules. Physicochemical properties such as aqueous solubility and lipophilicity play a determining role in drug absorption as well as pharmacokinetic profiles of molecules. A good HLB aids the molecule in passing through biological membranes and barriers to eventually enter the systemic circulation.[76,77] A traditional method for the evaluation of the druglikeness of a molecule is to check the compliance of "Lipinski's rule of five".[78,79] Calculated physicochemical properties of all of the synthesized compounds except the citrate salt were evaluated[80] to assess the compliance of Lipinski's rule of five (Table 2). Data showed that (a) all molecules are compliant with H-bonding properties, (b) all of the conjugate molecules have a log *P* in the range of 4−6, which may indicate that the molecules are lipophilic, (c) all of the conjugate molecules from the orthogonal and flexible series [except **1a** (MW: 499.52)]

Table 2. Calculated Physicochemical Properties of All Compounds

entry	MW[a]	log *D*[a] pH 7.4	log *P*[a]	no. of[a] H-bond donors	no. of[a] H-bond acceptors	no. of Lipinski violations
1a	499.52	5.36	5.37	0	5	2
1b	514.54	2.91	4.06	0	6	1
1c	551.56	3.94	4.01	0	6	1
1d	563.99	5.81	5.81	0	6	3
1e	579.01	3.36	4.51	0	7	1
2a	607.06	4.48	5.43	1	7	2
2b	622.08	2.03	4.12	1	8	1
2c	659.10	3.05	4.07	1	8	1
4	482.50	0.65	0.78	0	6	0
5	314.81	3.79	4.75	1	3	0
CQ	319.89	0.88	3.93	1	3	0

[a]All calculations were performed using MarvinSketch 5.8.1 from ChemAxon.

DOI: 10.1021/acsomega.6b00060
ACS Omega 2016, 1, 318−333

exhibit molecular weights slightly higher (in the range of 514−660) than the accepted value of 500, and (d) among all of the hybrid molecules **1a** and **1d** have log *D* values at pH 7.4 higher than 5.

Most active compounds (**2a** and **2b**), which have comparable activity (IC_{50} < 5 nM) against the CQ-sensitive strain, are almost compliant with Lipinski's rule of five with no. of violations two and one, respectively. Comparing H-bonding properties of Ac−en−NDI molecule **2c** with individual components **4** and **5**, it is evident that the number of H-bonding properties has been increased in conjugate **2c**. This increase in number of H-bonding properties may be attributed to the higher activity of conjugate molecules.

Plausible MOA of the Conjugate Molecules against *P. falciparum*. The existing knowledge about the mechanistic details of antimalarial action of Ac derivatives is limited despite findings suggesting Ac derivatives may target the inhibition of hemozoin (β-hematin) formation, mitochondrial bc1 complex, DNA topoisomerase II, and DNA gyrase.[24,65,81] NDI and naphthalimide derivatives have been used as relevant pharmacophores in anticancerous agents. The most consensual MOA of NDI and naphthalimide derivatives against different cancers is the interaction with DNA (ds DNA/G-quadruplex DNA).[42−45] Here, we have examined the MOA of flexible Ac−en−NDI **2a**, which is the most potent against the *Pf* 3D7 strain amongst the series of compounds studied by us.

The intraerythrocytic cycle of *P. falciparum* begins with the merozoite invasion of an erythrocyte, and it ends 48 h later when multiple new merozoites escape from the host cell. In the meantime, *Plasmodium* grows through ring (0−20 h post invasion (p.i)), trophozoite (20−36 h p.i), and schizont (36−48 h p.i) stages. To elucidate the MOA, we first evaluated the effect of **2a** at different stages of parasites to understand the stage-specific effects. Synchronized ring- (∼12 h p.i), trophozoite- (∼24 h p.i), and schizont-stage (∼36 h p.i) parasites were treated with 50 nM **2a** for 12 h. The parasites were washed to remove drug pressure and followed by incubation in drug-free complete media to complete the first life cycle. After completion of the first life cycle, the growth was determined using fluorescence-based SYBR Green I assay. Interestingly, the growth of parasites indicated that **2a** was more effective for the ring- and trophozoite-stage parasites with a moderate effect on the schizont-stage parasites (Figure 4). Compound **2a** exhibited ∼30% inhibition of growth at the schizont stage, whereas for ring and trophozoite stages, inhibition of growth was ∼80% (Figure 4). Interestingly, the effects of **2a** on ring- and trophozoite-stage parasites (12 h treatment) were similar to continuous treatment of **2a** in the complete cycle (36 h, beginning at the ring stage). Compound **2b** also exerts the same trend of growth inhibition (Figure S5). These results suggest that molecular targets common to both ring and trophozoite stages are affected by Ac−NDI conjugate molecules.

For instance, hemozoin formation, an essential process for the survival of parasites, starts at the ring stage and continues until the trophozoite stage. The process of hemozoin formation is linked with the hemoglobin digestion in the food vacuole, as the release of heme after hemoglobin digestion poses immediate demand for its detoxification. Trophozoite is the most active stage at digesting host cell hemoglobin and subsequent hemozoin formation.[82,83] The food vacuole of the late-trophozoite-stage parasite becomes full with hemozoin crystals, which can characterized microscopically. To find if

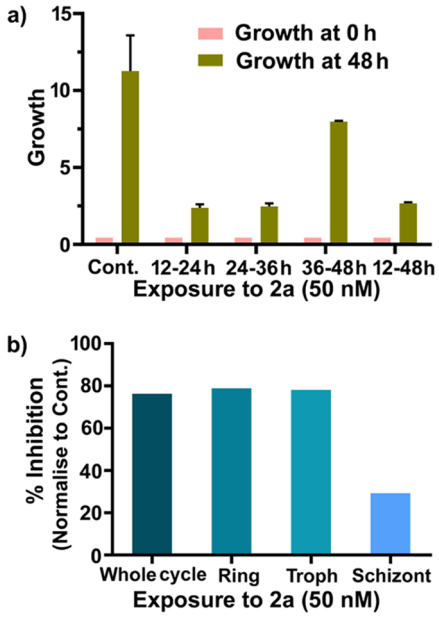

Figure 4. Effect of **2a** on different intraerythrocytic stages of malaria parasite *P. falciparum* (3D7). Highly synchronized ring (∼12 h), trophozoite (∼24 h), and schizont (∼36 h) stages were treated with 50 nM **2a** for 12 h. After completion of treatment, parasites were washed to remove drug pressure and subsequently resuspended in drug-free media to complete the life cycle. Ring-stage parasites (∼12 h) were also incubated continuously for 36 h. After completion of the first life cycle, the growth of the parasites was determined by fluorescence-based SYBR Green I assay. (a) Growth of different intraerythrocytic stages treated with **2a**. (b) Percentage inhibition of growth of different intraerythrocytic stages treated with **2a**. Data are presented as mean ± SEM from three independent experiments.

hemozoin formation may be a target for the antimalarial action of Ac−NDI conjugates, we assessed whether conjugates **2a** and **2b** might inhibit trophozoite development. Synchronized parasites at the midring stage (12 h p.i) were grown either in normal culture media (no drug) or media supplemented with 50 nM **2a**/**2b** or 5 μM CQ. Giemsa-stained smears were prepared from aliquots of the cultures at different time points. The morphology of the parasites was examined using a light reflecting microscope. As shown in Figure 5, compound **2a** and **2b** or CQ had a dramatic effect on the maturation of trophozoites. In all of the cases, ∼24 h treatment was sufficient enough to prevent the parasite development, and no hemozoin was seen in the food vacuole (Figure 5, **2a** 24 h, **2b** 24 h, and CQ 24 h). Parasite condensation and the appearance of pycnotic forms were observed with prolonged incubation of molecules **2a**/**2b** (Figure 5, **2a**/**2b** 48 h), contrasting with the shapeless uncondensed forms observed with CQ (Figure 5, CQ 48 h). Thus, our results indicate that Ac−NDI conjugates (**2a** and **2b**) prevent the trophozoite development possibly through inhibiting hemozoin formation.

To show that the antiplasmodial mechanism of Ac−NDIs may be because of the inhibition of the hemozoin formation, we decided to evaluate the binding of the most potent compound **2a** with heme using UV−vis spectroscopy. The sequential addition of small increments of **2a** into a constant concentration of monomeric heme solution of pH 7.5 resulted in a substantial decrease in the intensity of the Soret band of FPIX (Fe^{3+}) (heme) at 402 nm (Figure 6a). The resulting absorbance data were corrected for dilution and then analyzed

DOI: 10.1021/acsomega.6b00060
ACS Omega 2016, 1, 318−333

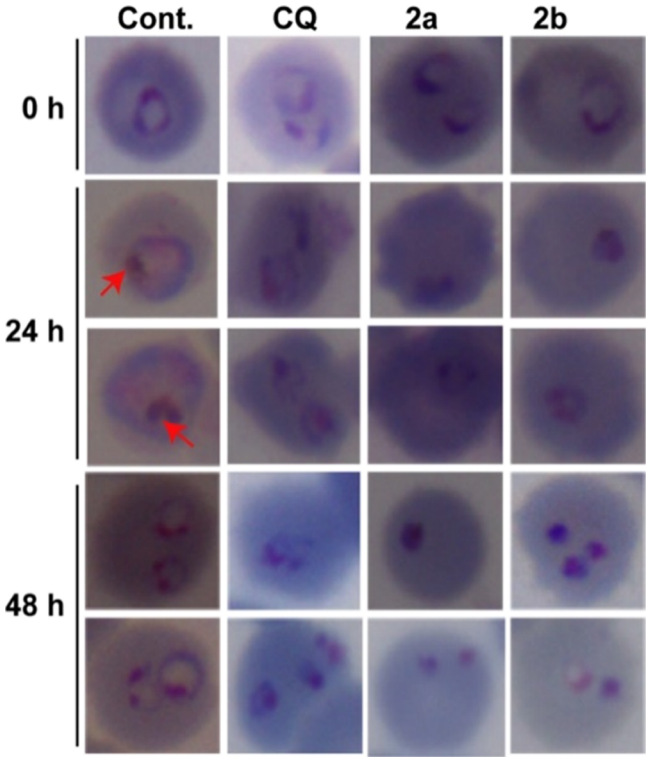

Figure 5. Inhibition of *P. falciparum* (3D7) trophozoite development. Synchronized ring-stage parasites (~12 h) of the intraerythrocytic cycle were grown either in the absence of any drug or in the presence of 5 μM CQ or 50 nM **2a**/**2b**. Giemsa-stained thin smears were microscopically examined at 0 h (~12 h-old parasite), 24 h (~36 h-old parasite), and 48 h (~60 h-old parasite). Compounds **2a**, **2b**, and **CQ** arrested the development of the trophozoite stage, and subsequently, no hemozoin formation was found in the treated parasite compared to the untreated (cont.) parasite. Red arrow indicates the hemozoin in the parasite food vacuole.

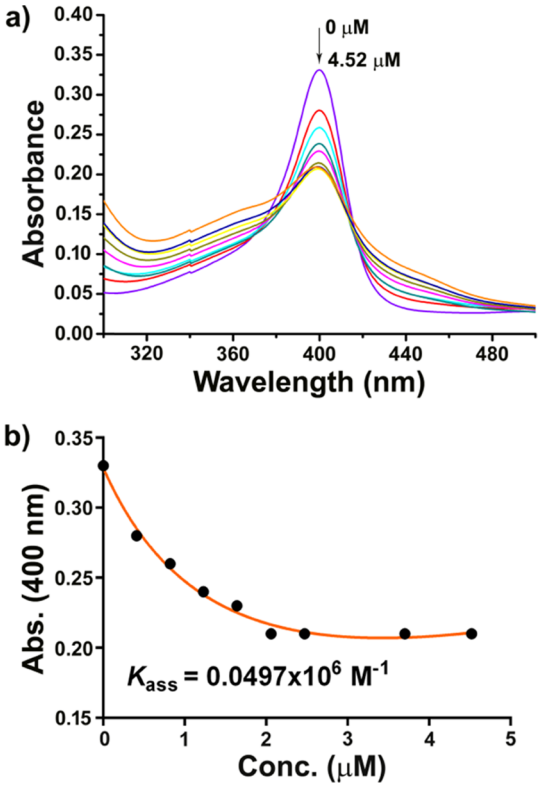

Figure 6. Binding of heme with compound **2a**. (a) Spectrophotometric titration of monomeric heme (2.4 μM) with increasing concentration of **2a** (0–4.52 μM in DMSO) at pH 7.4 (0.02 M HEPES buffer in aqueous DMSO). The decreasing band between 380 and 420 nm is characteristic of the heme. (b) Plot of absorbance at 400 nm against increasing concentration of **2a**. Nonlinear least-square fits of experimental data with the 1:1 binding model.

using nonlinear curve-fitting software to calculate the equilibrium binding constant of **2a** with monomeric heme. The best fit of the absorbance data was obtained with a 1:1 binding model (Figure 6b), which yielded a K_{ass} (association constant) value of 0.0497 × 10^6 M^{-1} (r^2 = 0.991). This result is in good agreement with the observation of Egan and co-workers that the 1:1 complex is predominant species in pH 7.5 *N*-(2-hydroxyethyl)piperazine-*N*′-ethanesulfonic acid (HEPES) buffer containing 40% dimethyl sulfoxide (DMSO).[84] Importantly, the association constant value of **2a** at pH 7.4 (log K_{ass} 4.70) is close to the reported value of the standard antimalarial drug CQ (log K_{ass} 5.15).[85]

The interaction of the Ac[67,81] and NDI[41−46] derivatives with DNA is well documented, and it is generally suggested that this interaction affects the activity of DNA metabolic enzymes such as topoisomerases. Recently, molecules such as quinone cyanine-dithiazole and thiazole-coumarin-based cell permeable fluorescence/NIR-fluorescence turn-ON probes specific toward AT-rich DNA were successfully applied for selective staining of the nucleus of an organism having an AT-rich genome, such as *P. falciparum*.[86,87] In this context, it is noteworthy that the conjugate **2a** failed to exhibit any significant interaction with DNA in UV−visible spectroscopy studies. The gradual addition of calf thymus (CT) DNA (0−7 × 10^{-4} M) to **2a** (~6 × 10^{-5} M) solution [3:1 MeOH:trisethelenediaminetetraacetic acid (TE) buffer (pH 8)] produced no significant changes in the absorption intensity as well as in the λ_{max} of **2a** (Figure S6). This noninteraction with DNA can be attributed to the bulkier size of conjugate molecule **2a**, which may not allow the Ac ring or NDI core to intercalate in between DNA base pairs. However, we were unable to employ a higher concentration of **2a** in the DNA interaction study by UV−visible spectroscopy because of precipitation.

Next, we evaluated the redox potential of orthogonal Ac−NDI **1a** and the most potent **2a** with the aid of cyclic voltammetry (CV) and differential pulse voltammetry (DPV) (Figure 7). Both molecules exhibited two well-separated reversible reduction waves. Molecules **1a** and **2a** showed first reduction potentials (E^1_{red}) at −0.48 and −0.51 V, respectively, and second reduction potentials (E^2_{red}) at −0.98 and −0.95 V, respectively, versus the saturated calomel electrode (SCE). From the comparison of E^1_{red} values of **2a** with **1a**, it becomes clearly evident that the linker between Ac and NDI decreases the π acidity of the NDI core in **2a**, which leads to the cathodically shifted reduction potential of **2a**.

Biological reductants such as glutathione (GSH) and nicotinamide adenine dinucleotide phosphate (NADPH) play pivotal role in maintaining the redox balance (redox homeostasis) in the parasite by providing reducing equivalents to the biosynthetic reactions involved in neutralizing ROS. Therefore, the depletion of these essential biological reductants inside of the parasite would cause the disruption of redox balance of the parasite, which in turn leads to the death of the parasite. The successful electrochemical reduction of Ac−en−NDI conjugate

DOI: 10.1021/acsomega.6b00060
ACS Omega 2016, 1, 318−333

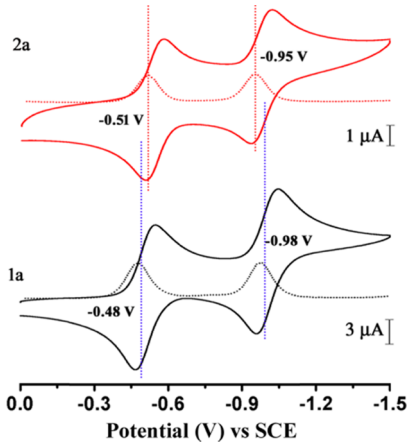

Figure 7. Cyclic voltammograms (CVs) of **1a** and **2a** in DMF with *n*-Bu_4NPF_6 as the electrolyte and a saturated calomel reference electrode, platinum working electrode, and auxiliary electrode.

2a prompted us to determine whether **2a** could be reduced in the presence of biological reductants. Sulfide (S^{2-}) was chosen as a model biological reductant for our study because of its favorable solubility in DMF over GSH; however, both S^{2-} and GSH have more positive physiological half-cell reaction reduction potentials[88] ∼+0.17, ∼−0.25 V, respectively, compared to **2a**. UV−visible spectroscopy of **2a** exhibited two strong absorption peaks at 361 and 378 nm because of the $\pi-\pi^*$ transitions for the NDI core. In the presence of S^{2-}, new signature peaks, characteristic of the radical anion $2a^{\bullet-}$, appeared at 475, 607, 682, and 757 nm with a concomitant decrease of the $\pi-\pi^*$ 361 and 378 nm bands (Figure 8). These

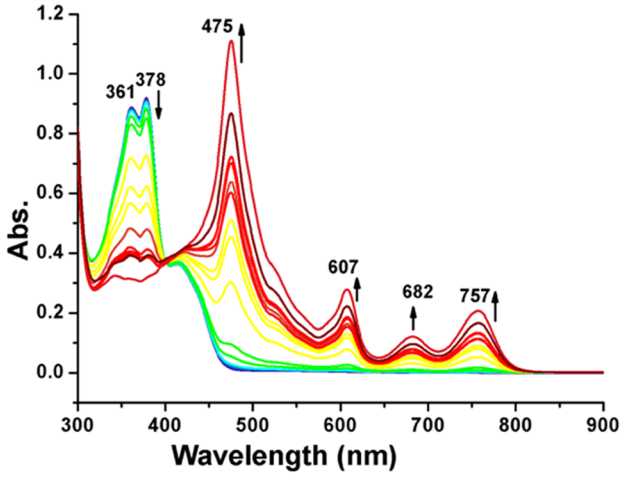

Figure 8. UV−vis spectra showing the reduction of **2a** (5×10^{-5}) upon incremental addition of S^{2-} (0−8 equiv) in DMF.

absorption bands as a result of the $D_0 \rightarrow D_n$ transitions corroborated the reduction of the NDI core. This result suggests that conjugate **2a** has a potential to interact with the biological reductant present in the parasite because of its redox property and thereby disrupt the redox balance of the parasite.

Owing to the similarity of redox properties of the NDI scaffold present in the Ac−NDI conjugate with mETC inhibitor atovaquone, we anticipated that Ac−NDIs may also interfere with the mETC and lead to mitochondrial dysfunction. We therefore examined whether **2a** could lead to the loss of the mitochondrial membrane potential ($\Delta\Psi_m$) in parasites. The $\Delta\Psi_m$ was determined using a membrane-potential-sensitive dye, JC-1, also known as 5,5′,6,6′-tetrachloro-1,1′,3,3′-tetraethylbenzimida-zolocarbocyanine iodide. JC-1 emits green fluorescence at 525 nm in its monomeric form. However, upon accumulation into intact healthy mitochondria with higher $\Delta\Psi_m$, it forms J aggregate and exhibits orange-red fluorescence at 590 nm. JC-1 accumulation would be less in the damaged mitochondria with low $\Delta\Psi_m$ and does not form aggregates because of its less availability and exhibits weak fluorescence at 590 nm. Synchronized midring-stage parasites (∼18 h p.i) were incubated with **2a** for 12, 24, and 36 h prior to 30 min incubation with JC-1. Fluorescence microscopic studies were carried out to measure the JC-1 accumulation ($\Delta\Psi_m$) in the presence or absence of **2a**. In the control (untreated) parasites, $\Delta\Psi_m$ increased as the parasite progressed from ring to trophozoite (12 h) and schizont (24 h) stages. However, $\Delta\Psi_m$ decreased dramatically as the parasites reached the next cycle (36 h) (Figure 9). The $\Delta\Psi_m$ value is proportional to the size of the mitochondrion, which increases gradually from ring to trophozoite and schizont stages. Further, the ratios of J aggregates to the monomer in the control (no drug) parasites were higher compared to those of parasites treated with **2a** for 12, 24, and 36 h (Figure 9). The observed red fluorescence (J aggregates) in parasites treated with **2a** (25 and 50 nM) for 12, 24, and 36 h was almost negligible or null compared to that in control parasites. Moreover, a minimum 12 h exposure to 25 nM **2a** was sufficient enough to disrupt the mitochondrial membrane potential as a considerably less amount of J-aggregate (red fluorescence) formation was observed within 12 h of exposure of 25 nM **2a**. These results clearly indicate that Ac−NDI conjugate **2a** disrupts the mitochondrial membrane potential in the malaria parasite and also suggest that mitochondrion is one of the targeting sites.

CONCLUSIONS

In this investigation, we have conjugated for the first time Ac and NDI pharmacophores through a facile condensation approach of primary amines with acid anhydride. These Ac−NDI conjugates were found to provide a new class of redox-active, electronically segmented NDI-based bifunctional antimalarial molecules against CQ-sensitive and CQ-resistant strains of *P. falciparum*. The in vitro evaluation of these conjugates against *Pf* 3D7 and *Pf* W2 strains depicted the activity of orthogonal Ac−NDI series (**1a−e**) in a micromolar to submicromolar range and flexible Ac−en−NDI series (**2a−c** and **3**) in a nanomolar range. Amongst the flexible Ac−en−NDI molecules, **2a** and **2b** were found to be most potent with IC_{50} values of 3.65 and 4.33 nM, respectively, against *Pf* 3D7. Significantly, against the *Pf* W2 strain, **2a** and **2b** exhibited IC_{50} values of 52.20 and 28.53 nM, respectively, which were around 1 order of magnitude better than those of the standard drug CQ. The SAR studies revealed that the amino ethyl spacer between Ac and NDI pharmacophores was critical to exhibit potent antiplasmodial activity. The evaluation of theoretical physicochemical properties suggested that conjugates **2a** and **2b** were almost compliant with Lipinski's rule of five with no. of violations two and one, respectively. Also, these potent conjugates were found to be low cytotoxic against mammalian cell lines. Further, to shed light on the MOA of these hybrids, our data suggests that (i) Ac−NDI binds to free heme, which may lead to an inhibition of hemozoin formation, (ii) the NDI scaffold in the conjugate molecule can uptake electrons from biological reductants, which may cause a depletion of essential

DOI: 10.1021/acsomega.6b00060
ACS Omega 2016, 1, 318−333

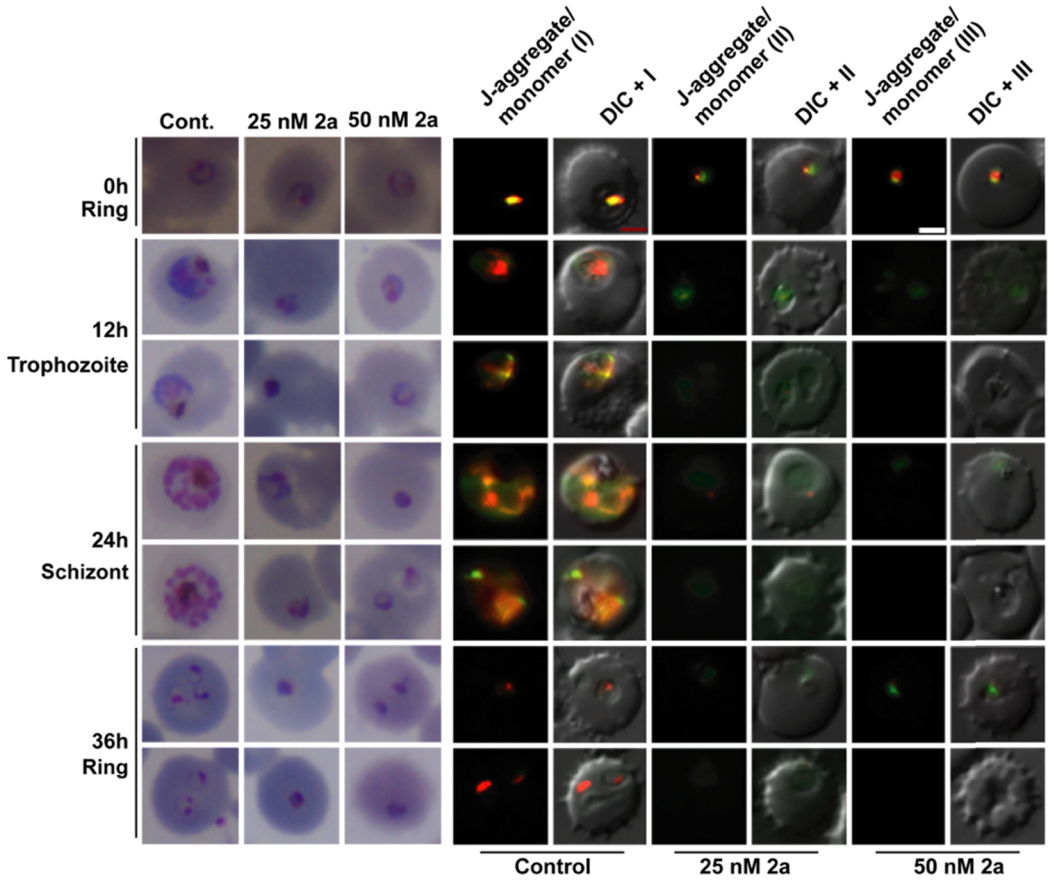

Figure 9. Dissipation of the mitochondrial membrane potential ($\Delta\Psi_m$) in the *P. falciparum* (3D7) parasite by the Ac−NDI hybrid. (a) Light microscopy images of Giemsa-stained smears to show the growth during developmental stages in untreated (control) and treated (25 and 50 nM **2a**) parasites. (b) Fluorescence microscopic analysis of JC-1-stained parasites to assess $\Delta\Psi_m$ during developmental stages in untreated (control) and treated (25 and 50 nM **2a**) parasites. Panels I, III, and V stand for the J aggregate (emission, 590 nm)/JC-1 monomer (emission, 525 nm) (merged). Panels II, IV, and VI stand for DIC + merged. High $\Delta\Psi_m$ in control mitochondria causes the J aggregation of JC-1, which leads to red-orange fluorescence. An exposure of parasites to **2a** leads to a significant decrease in J-aggregate formation as indicated by a switch of red-orange fluorescence (control, I) to green fluorescence (treated, III and IV), demonstrating a collapse of $\Delta\Psi_m$. The scale bar is 2 μm.

biological reducing equivalents inside of the parasite and thereby affecting the redox equilibrium of the parasite, and (iii) Ac−NDI causes the disruption of the mitochondrial membrane potential. Therefore, the proposed antiplasmodial MOA of these molecules is quite distinct from that of CQ- and Ac-based antimalarials and also clearly suggests that the biofunctional activity of these Ac−NDI conjugates to produce antimalarial activity. Overall, our data demonstrate that the NDI scaffold in the Ac−NDI bifunctional molecule plays significant role(s) in intervening various biological pathways leading to the parasitic death.

EXPERIMENTAL SECTION

General. All of the chemicals (starting materials and reagents for synthesis) were procured from the following companies: Fluka, Sigma-Aldrich, Spectrochem, India, and Thomas Baker, India. Freshly distilled and dry solvents were used in reactions under an anhydrous nitrogen atmosphere. Reactions were monitored by thin layer chromatography (TLC) on precoated silica gel 60 F254 (0.25 mm, Merck). Flash chromatography was performed in silica gel (100−200 mesh). Elemental analysis was carried out with a Perkin-Elmer/Thermo Scientific elemental analyzer. NMR (^{1}H, ^{13}C, DEPT-135 and APT) spectra were recorded on a Bruker 500 MHz spectrometer using tetramethylsilane (TMS) as the internal standard in $CDCl_3$ or DMSO-d_6 or MeOH-d_4. MALDI-TOF mass spectra were recorded on a Bruker Autoflex TOF/TOF instrument with a laser repetition rate of 50 ps. Either α-cyano-4-hydroxycinnamic acid or 1,8,9-anthracenetriol was used as the matrix for MALDI-TOF mass spectrometry. IR spectra (KBr pellet) were recorded on a Varian 3100 FT-IR spectrophotometer. UV−visible spectroscopic studies were carried out on a JASCO, V-670 model spectrophotometer with a 1 cm path length quartz cuvette.

Synthesis of 1a. 9-Aminoacridine hydrochloride (0.523 g, 2.1 mmol), butyl amine (0.189 mL, 1.90 mmol), and triethyl amine (0.530 mL, 3.8 mmol) were transferred to a 100 mL round-bottom flask containing 1,4,5,8-napthalenetetracarboxylic dianhydride (0.50 g, 1.86 mmol) in 25 mL of DMF in a N_2 atmosphere. The reaction mixture was heated on a magnetic stirrer at 140 °C for 5 h and cooled to room temperature (RT). The reaction mixture was completely dried under vacuum. The solid material obtained was dissolved in chloroform and filtered; the filtrate was dried by vacuum rotary evaporation, and a solid crude product was obtained. Further purification of the above crude product was carried out by preparative TLC (silica gel G, $CHCl_3$). Yield: 53 mg (5.68%). R_f = 0.87 (9:1 $CHCl_3$/MeOH). Mp: >300 °C. ^{1}H NMR (500 MHz, $CDCl_3$, 298 K, TMS): δ = 8.88 (m, 4H, *Nap*), 8.39 (d, 2H, J = 9 MHz, *Acr*), 7.81 (m, 4H, *Acr*), 7.54 (m, 2H, *Acr*), 4.28 (t, J = 8 MHz,

DOI: 10.1021/acsomega.6b00060
ACS Omega 2016, 1, 318−333

2H, NCH_2−), 1.79 (m, 2H, −$CH_2CH_2CH_2$−), 1.11 (2H, −CH_2CH_3), 1.03 (t, J = 7.5 MHz, 3H, −CH_2CH_3). ^{13}C NMR (125 MHz, $CDCl_3$, 298 K, TMS): δ = 162.66, 149.01, 138.04, 132.01, 131.79, 131.04, 130.43, 129.37, 127.83, 127.59, 127.55, 127.49, 127.45, 127.03, 126.99, 126.84, 125.97, 125.93, 123.46, 122.07, 61.34, 40.87, 30.74, 30.10, 29.61, 29.29, 27.45, 27.29, 25.34, 22.67, 20.26, 13.99, 13.70. MS (MALDI-TOF matrix: α-cyano-4-hydroxycinnamic acid): calculated for $C_{31}H_{21}N_3O_4$ (m/z) 499.52, found 500.21. FTIR (KBr Pellet): ν (cm^{-1}) = 2921, 2850, 1720, 1706, 1683, 1663, 1581. Anal. Calcd for $C_{31}H_{21}N_3O_4$: C, 75.54; H, 4.24; N, 8.41. Found: C, 75.43; H, 4.12; N, 8.53.

Synthesis of 1b. 9-Aminoacridine hydrochloride (0.523 g, 2.1 mmol), *N*,*N*-dimethylethelynediamine (0.208 mL, 1.90 mmol), and triethyl amine (0.530 mL, 3.8 mmol) were transferred to a 100 mL round-bottom flask containing 1,4,5,8-napthalenetetracarboxylic dianhydride (0.50 g, 1.86 mmol) in 25 mL of DMF in a N_2 atmosphere. The reaction mixture was heated on a magnetic stirrer at 140 °C for 5 h and cooled to RT. The reaction mixture was completely dried under vacuum. The solid material obtained was dissolved in chloroform and filtered; the filtrate was dried by vacuum rotary evaporation, and a solid crude product was obtained. Further purification of the above crude product was carried out by preparative TLC (silica gel G, $CHCl_3$/MeOH (35.7:1). Yield: 67 mg (7.0%). R_f = 0.56 (9:1 $CHCl_3$/MeOH). Mp: 284 °C. ^{1}H NMR (500 MHz, $CDCl_3$, 298 K, TMS): δ = 8.75 (4H, *Nap*), 8.28 (q, 2H, J = 4.5 Hz, *Acr*), 7.73 (m, 4H, *Acr*), 7.45 (m, 2H, *Acr*), 4.35 (t, 2H, J = 6 MHz, NCH_2−), 2.80 (b, 2H, −CH_2−), 2.39 (s, 6H, N(CH_3)$_2$). ^{13}C NMR (125 MHz, $CDCl_3$, 298 K, TMS): δ = 163.00, 162.61, 149.63, 137.30, 131.96, 131.25, 130.50, 127.72, 127.62, 127.53, 127.23, 126.16, 123.38, 122.01, 56.71, 45.43, 38.175. MS (MALDI-TOF matrix: α-cyano-4-hydroxycinnamic acid): calculated for $C_{31}H_{22}N_4O_4$ (m/z) 514.53, found 515.19. FTIR (KBr pellet): ν (cm^{-1}) = 2944, 2817, 1707, 1666, 1578, 1335. Anal. Calcd for $C_{31}H_{22}N_4O_4$: C, 72.36; H, 4.31; N, 10.89. Found: C, 72.42; H, 4.45; N, 10.76.

Synthesis of 1c. 9-Aminoacridine hydrochloride (0.694 g, 2.8 mmol), 1-(3-aminopropyl)imidazole (0.222 mL, 1.86 mmol), and triethyl amine (0.392 mL, 2.8 mmol) were transferred to a 100 mL round-bottom flask containing 1,4,5,8-napthalenetetracarboxylic dianhydride (0.50 g, 1.86 mmol) in 25 mL of DMF in a N_2 atmosphere. The reaction mixture was heated on a magnetic stirrer at 140 °C for 6.5 h and cooled to RT. The reaction mixture was filtered to remove the unreacted 9-aminoacridine. Cold diethyl ether was added to the filtrate and precipitation occurred. The solid material was separated and completely dried under vacuum. Further purification of the above crude product was carried out by preparative TLC (silica gel G, $CHCl_3$/MeOH/Et_3N (50:1:0.1). Yield: 27 mg (15.25%). R_f = 0.476 (9:1 $CHCl_3$/MeOH). Mp: 305 °C (decomposed). ^{1}H NMR (500 MHz, MeOD, 298 K, TMS): δ = 8.87 (s, 4H, *Nap*), 8.34 (d, 2H, J = 9 Hz, *Acr*), 7.92 (m, 4H, *Acr*), 7.69 (s, 1H, *Imz*), 7.614 (dd-merged, 2H, *Acr*), 7.16 (s, 1H, *Imz*), 6.98 (s, 1H, *Imz*), 4.32 (t, J = 7 Hz, 2H, −CH_2Imz), 4.22 (t, J = 7 Hz, N−CH_2−CH_2−), 2.36 (m, 2H, −CH_2−CH_2−CH_2−). ^{13}C NMR (125 MHz, $CDCl_3$, 298 K, TMS): δ = 162.93, 162.79, 149.10, 138.33, 137.09, 131.80, 131.14, 131.07, 128.99, 128.26, 127.76, 127.70, 127.30, 127.10, 126.26, 123.58, 122.31, 119.09, 44.906, 38.188, 31.46, 29.09, 13.62. MS (MALDI-TOF matrix: α-cyano-4-hydroxycinnamic acid): calculated for $C_{33}H_{21}N_5O_4$ (m/z) 551.55, found 551.22. FTIR (KBr pellet): ν (cm^{-1}) = 2924, 1704, 1668, 1578, 1333. Anal. Calcd for $C_{33}H_{21}N_5O_4$: C, 71.86; H, 3.84; N, 12.70. Found: C, 71.71; H, 3.75; N, 12.56.

Synthesis of 1d. 6-Chloro-2-methoxy-9-aminoacridine (0.492 g, 1.9 mmol) and *n*-butylamine (0.189 mL, 1.90 mmol) were transferred to a 100 mL round-bottom flask containing 1,4,5,8-napthalenetetracarboxylic dianhydride (0.50 g, 1.86 mmol) in 25 mL of DMF in a N_2 atmosphere. The reaction mixture was heated on a magnetic stirrer at 140 °C for 5 h and cooled to RT followed by filtration to remove the precipitate (bis Ac and bis alkyl product). DMF was removed from the filtrate under reduced pressure to obtain the solid material. The solid material was washed with methanol (3 × 30 mL) and completely dried under vacuum. Further purification of the above crude product was carried out by flash column chromatography on silica gel (100:0 to 100:0.5 $CHCl_3$/MeOH) to yield the product as a yellow solid. Yield: 112 mg (32%). R_f = 0.60 (9:1 $CHCl_3$/MeOH). Mp: 300 °C (decomposed). ^{1}H NMR (500 MHz, $CDCl_3$, 298 K, TMS): δ = 8.87 (4H, *Nap*), 8.33 (s, 1H, *Acr*), 8.26 (d, J = 9 Hz, 1H, *Acr*), 7.64 (d, J = 9 Hz, 1H, *Acr*), 7.54 (d, J = 9.5 Hz, 1H, *Acr*), 7.43 (d, J = 9 Hz, 1H, *Acr*), 6.78 (s, 1H, *Acr*), 4.26 (2H, −NCH_2−), 3.73 (s, 3H, CH_3O), 1.76 (2H, $CH_2CH_2CH_2$), 1.49 (2H, $CH_2CH_2CH_3$), 1.02 (t, J = 6.5 MHz, 3H, CH_2CH_3). ^{13}C NMR (125 MHz, $CDCl_3$, 298 K, TMS): δ = 162.61, 162.38, 158.98, 147.76, 177.72, 135.20, 135.00, 132.24, 132.13, 131.25, 129.01, 128.96, 127.65, 127.15, 126.20, 125.92, 124.67, 122.90, 121.99, 97.26, 55.56, 40.94, 30.19, 22.65, 20.37, 13.85.MS (MALDI-TOF matrix: 1,8,9-anthracenetriol): calculated for $C_{32}H_{22}ClN_3O_5$ (m/z) 563.99 found 564.15. FTIR (KBr Pellet) ν (cm^{-1}) = 3084, 2960, 2930, 2866, 1710, 1667, 1631, 1580, 1472, 1338. Anal. Calcd for $C_{32}H_{22}ClN_3O_5$: C, 68.15; H, 3.93; N, 7.45. Found: C, 68.24; H, 3.85; N, 7.52.

Synthesis of 1e. 6-Chloro-2-methoxy-9-aminoacridine (0.492 g, 1.9 mmol) and *N*,*N*-dimethylethelynediamine (0.208 mL, 1.90 mmol) were transferred to a 100 mL round-bottom flask containing 1,4,5,8-napthalenetetracarboxylic dianhydride (0.50 g, 1.86 mmol) in 25 mL of DMF in a N_2 atmosphere. The reaction mixture was heated on a magnetic stirrer at 140 °C for 5 h and cooled to RT. DMF was removed from the reaction mixture under reduced pressure. The solid material was completely dried under vacuum. Further purification of the above crude product was carried out by flash column chromatography on silica gel (100:0 to 100:4 $CHCl_3$/MeOH) to yield the product as a yellow solid. Yield: 21 mg (15.43%). R_f = 0.45 (9:1 $CHCl_3$/MeOH). Mp: 310 °C. ^{1}H NMR (500 MHz, $CDCl_3$, 298 K, TMS): δ = 8.86 (4H, *Nap*), 8.32 (1H, *Acr*), 8.22 (d, J = 9 Hz, 1H, *Acr*), 7.64 (d, J = 8.5 Hz, 1H, *Acr*), 7.51 (d, J = 8.5 Hz, 1H, *Acr*), 7.44 (d, J = 8.5 Hz, 1H, *Acr*), 6.78 (s, 1H, *Acr*), 4.41 (2H, −NCH_2CH_2−), 3.73 (s, 3H, −OCH_3), 2.72 (2H, −CH_2N), 2.35 (s, 6H, (CH_3)$_2$N−). ^{13}C NMR (125 MHz, $CDCl_3$, 298 K, TMS): δ = 162.71, 162.39, 158.99, 147.76, 135.20, 132.23, 131.29, 129.01, 127.64, 127.23, 126.13, 125.94, 124.67, 122.91, 121.99, 97.23, 56.98, 55.57, 45.86, 38.81. MS (MALDI-TOF matrix: α-cyano-4-hydroxycinnamic acid): calculated for $C_{32}H_{23}ClN_4O_5$ (m/z) 579.14, found 579.30. FTIR (KBr Pellet) ν (cm^{-1}) = 3077, 2944, 2825, 2770, 1710, 1670, 1631, 1579, 1330. Anal. Calcd for $C_{32}H_{23}ClN_4O_5$: C, 66.38; H, 4.00; N, 9.68. Found: C, 66.49; H, 4.11; N, 9.56.

Synthesis of 2a. A 100 mL round-bottom flask containing 1,4,5,8-napthalenetetracarboxylic dianhydride (0.50 g, 1.86 mmol), *N*-(2-aminoethyl)-3-chloro-2-methoxyacridine-9-amine (0.63 g, 2.09 mmol), and butyl amine (227 μL, 2.09 mmol) in 25 mL of dry DMF were heated on a magnetic stirrer at 140 °C

DOI: 10.1021/acsomega.6b00060
ACS Omega 2016, 1, 318−333

for 2 h under a N_2 atmosphere. The reaction mixture was gradually brought to RT. This solution was added to 50 mL of diethyl ether to precipitate out a green-colored solid material. The solid material was separated by filtration and completely dried under vacuum. The solid material was purified by flash column chromatography on silica gel (100:0 to 100:2.5 $CHCl_3$/MeOH) to yield the product as a yellow solid. Yield: 94 mg (25%). R_f = 0.71 (9:1 $CHCl_3$/MeOH). Mp: 160 °C. ^{1}H NMR (500 MHz, $CDCl_3$, 298 K, TMS): δ = (d, J = 8 Hz, 2H, *Nap*), 8.50 (d, 2H, J = 7.5 Hz, *Nap*), 7.93 (d, J = 9.5 Hz, 1H, *Acr*), 7.68 (s, 1H, *Acr*), 7.64 (d, J = 9.5 Hz, 1H, *Acr*), 7.20 (m, 1H, *Acr*), 7.10 (m, 2H, *Acr*), 5.68 (s, 1H, −*NH*), 4.56 (t, 2H, J = 5 Hz, CH_2−NH−), 4.16 (s, 2H, −CH_2N), 4.08 (t, J = 7.5 Hz, 2H, −NCH_2), 4.00 (s, 3H, −OCH_3), 1.61 (m, 2H, −NCH$_2$$CH_2CH_2$−), 1.36 (m, 2H, −CH$_2$$CH_2CH_3$), 0.90 (t, J = 7.5 Hz, 3H, −CH$_2$$CH_3$). ^{13}C NMR (125 MHz, $CDCl_3$, 298 K, TMS): δ = 163.84, 162.50, 156.03, 148.93, 148.38, 146.16, 134.61, 131.11, 130.74, 127.98, 127.01, 126.50, 125.56, 124.53, 124.02, 116.61, 114.26, 98.56, 55.65, 49.20, 41.71, 30.10, 20.33, 13.80. MS (MALDI-TOF matrix: α-cyano-4-hydroxycinnamic acid): calculated for $C_{34}H_{27}ClN_4O_5$ (m/z) 607.05, found 607.02. FTIR (KBr pellet): ν (cm^{-1}) = 3412, 2962, 2932, 2870, 1705, 1663, 1573, 1519, 1453, 1334. Anal. Calcd for $C_{34}H_{27}ClN_4O_5$: C, 67.27; H, 4.48; N, 9.23. Found: C, 67.36; H, 4.38; N, 9.35.

Synthesis of 2b. *N*,*N*-Dimethylethelynediamine (208 μL, 1.9 mmol) was transferred to a 100 mL round-bottom flask containing 1,4,5,8-naphthalenetetracarboxylic dianhydride (0.50 g, 1.86 mmol) and *N*-(2-aminoethyl)-3-chloro-2-methoxyacridine-9-amine (0.302 g, 1.9 mmol) in 25 mL of DMF in a N_2 atmosphere. The reaction mixture was heated on a magnetic stirrer at 140 °C for 3 h. The reaction mixture was gradually brought to RT; 50 mL of cold diethyl ether was added. The green precipitate was filtered and dried under vacuum. The crude material was purified by flash column chromatography on silica gel (100:0 to 96:4 $CHCl_3$/MeOH) to yield the product as a yellow solid. Yield: 72 mg (18%). R_f = 0.42 (9:1 $CHCl_3$/MeOH). Mp: 155 °C. ^{1}H NMR (500 MHz, $CDCl_3$, 298 K, TMS): δ = 8.70−8.54 (m, 4H, *Nap*), 8.02−8.00 (1H, *Acr*), 7.68−7.67 (1H, *Acr*), 7.24−7.15 (m, 3H, *Acr*), 4.59 (s, 2H, −CH_2NH−), 4.27−4.20 (4H, 2(CH_2−*N*−)), 4.02 (s, 3H, −OCH_3), 2.62 (s, 2H, −NH−CH$_2$$CH_2CH_2$N−), 2.28 (s, 6H, N($CH_3$)$_2$). ^{13}C NMR (125 MHz, $CDCl_3$, 298 K, TMS): δ = 163.84, 162.62, 156.02, 148.97, 148.38, 146.13, 134.65, 131.10, 130.83, 127.96, 126.98, 126.56, 125.57, 124.57, 124.04, 116.60, 114.25, 98.64, 56.92, 55.67, 49.18, 45.82, 41.74, 38.71. MS (MALDI-TOF matrix: α-cyano-4-hydroxycinnamic acid): calculated for $C_{34}H_{28}N_5O_5$ (m/z) 621.18, found 622.41. FTIR (KBr pellet): ν (cm^{-1}) = 3388, 2950, 2828, 2778, 1705, 1662, 1569, 1335. Anal. Calcd for $C_{34}H_{28}N_5O_5$: C, 65.65; H, 4.54; N, 11.26. Found: C, 65.53; H, 4.63; N, 11.34.

Synthesis of 2c. 1-(3-Aminopropyl)imidazole (227 μL, 1.9 mmol) was transferred to a 100 mL round-bottom flask containing 1,4,5,8-naphthalenetetracarboxylic dianhydride (0.50 g, 1.86 mmol) and *N*-(2-aminoethyl)-3-chloro-2-methoxyacridine-9-amine (0.302 g, 1.9 mmol) in 25 mL of DMF in a N_2 atmosphere. The reaction mixture was heated on a magnetic stirrer at 140 °C for 3 h. The reaction mixture was gradually brought to RT; 50 mL of cold diethyl ether was added. The green precipitate was filtered and dried under vacuum. The crude material was purified by preparative TLC (silica gel G, $CHCl_3$/MeOH (96:4)) to yield the product as a yellow solid. Yield: 25 mg (6%). R_f = 0.47 (9:1 $CHCl_3$/MeOH). Mp: 250 °C (decomposed). ^{1}H NMR (500 MHz, $CDCl_3$, 298 K, TMS): δ = 8.70 (d, J = 7.5 Hz, 2H, *Nap*), 8.56 (d, J = 7.5 Hz, 2H, *Nap*), 8.00 (d, J = 9.5 Hz, 1H, *Acr*), 7.78 (s, 1H, *Ar*), 7.698 (s (b), 1H, *Ar*), 7.47 (s, 1H, *Ar*), 7.19 (m, 2H, *Ar*), 6.93 (m, 3H, *Ar*), 4.62 (s, 1H, *HN*-Acr), 4.21 (m, 4H, 2(CH_2−*N*−)), 4.03 (m, 7H, 2(CH_2−*N*−) & −OCH_3), 2.17 (m, 2H, −CH$_2$$CH_2CH_2$). ^{13}C NMR (125 MHz, $CDCl_3$, 298 K, TMS). Because of very poor solubility of the compound in $CDCl_3$/DMSO-d_6, we failed to get a reasonable S/N even up to 10K scan. MS (MALDI-TOF matrix: α-cyano-4-hydroxycinnamic acid): calculated for $C_{36}H_{27}ClN_6O_5$ (m/z) 659.09, found 659.28. FTIR (KBr pellet): ν (cm^{-1}) = 3390, 2963, 1703, 1662, 1570, 1337. Anal. Calcd for $C_{36}H_{27}ClN_6O_5$: C, 65.60; H, 4.13; N, 12.75. Found: C, 65.52; H, 4.18; N, 12.61.

Synthesis of 3. To a solution of **2a** (20 mg, 0.03 mmol) in anhydrous MeOH (5 mL) was added a solution of citric acid (6.33 mg, 0.03 mmol) in anhydrous MeOH (1 mL). The corresponding citrate salt precipitated spontaneously, and then, the resulting suspension was left for 1 day at RT until complete precipitation. After the removal of the solvent, the solid residue was washed with MeOH and then with acetone and dried under vacuum, affording the desired citrate salt. Yield: 24 mg (91%). Mp: 200 °C (decomposed). ^{1}H NMR (500 MHz, DMSO-d_6, 298 K, TMS): δ = 8.57 (d, J = 7.5 Hz, 2H, *Nap*), 8.43 (d, J = 9 Hz, 1H, *Acr*), 8.38 (d, J = 7.5 Hz, 2H, *Nap*), 7.60 (s, 1H, *Acr*), 7.54−7.51 (m, 2H, *Acr*), 7.43 (1H, *Acr*), 7.35 (d, J = 9 Hz, 1H, *Acr*), 4.45 (2H, *NH*), 4.34 (2H, −HNCH_2CH$_2$−), 4.05 (t, J = 7.5 Hz, 4H, NCH_2CH$_2$−), 3.86 (s, 3H, −OCH_3), 2.65−2.64 (2H, −CH_2−citrate), 2.62−2.569 (2H, −CH_2−citrate), 1.64−1.60 (m, 2H, −CH$_2$$CH_2CH_3$), 0.92 (t, J = 7.5 Hz, 3H, −CH$_2$$CH_3$).

Synthesis of 4. 1-(3-Aminopropyl)imidazole (0.806 mL, 5.70 mmol) was transferred to a 50 mL round-bottom flask containing 1,4,5,8-napthalenetetracarboxylic dianhydride (0.50 gm, 1.86 mmol) in 25 mL of DMF in a N_2 atmosphere. The reaction mixture was heated on a magnetic stirrer at 140 °C for 5 h and cooled to RT. Ice-cold water was added to the solution to precipitate out the product. The precipitate was separated by filtration and dried under vacuum. Further purification of this crude solid was carried out by flash column chromatography on silica gel using $CHCl_3$/MeOH as an eluent (MeOH gradient 0−2%) and afforded a yellow solid product. Yield: 0.272 gm (29.67%). R_f = 0.51 (9:1 $CHCl_3$/MeOH). Mp: 280 °C (decomposed). ^{1}H NMR (500 MHz, DMSO-d_6, 298 K, TMS): δ = 8.66 (s, 4H, *Nap*), 7.67 (s, 2H, *Imz*), 7.22 (s, 1H, *Imz*), 6.87 (s, 1H, *Imz*), 4.08 (m, 8H, NCH_2−), 2.12 (m, 4H, 2(CH$_2$$CH_2CH_2$)). ^{13}C NMR (125 MHz, DMSO-d_6, 298 K, TMS): δ = 163.26, 137.71, 130.83, 128.81, 126.81, 119.70, 44.52, 38.26, 29.63. MS (MALDI-TOF matrix: 1,8,9-anthracenetriol): calculated for $C_{26}H_{22}N_6O_4$ (m/z) 482.49, found 483.15. FTIR (KBr pellet): ν (cm^{-1}) = 3106, 3068, 2948, 2924, 2849, 1705, 1656, 1578, 1508, 1456. Anal. Calcd for $C_{26}H_{22}N_6O_4$: C, 64.72; H, 4.60; N, 17.42. Found: C, 64.64; H, 4.51; N, 17.56.

Synthesis of 5. 6,9-Dichloro-2-methoxyacridine (0.250 g, 0.9 mmol) was dissolved in butyl amine (5 mL) and stirred at 80 °C for 4 h and cooled to RT. The solution was added to 30 mL of water and extracted with DCM. The organic layer was washed with brine solution (50 mL × 3) and dried over anhydrous $MgSO_4$, and the solution was evaporated using a rotary evaporator. The crude residue was subjected to column chromatography on silica gel (100:0 to 96:4 $CHCl_3$/MeOH) to get the product as a yellow solid. Yield: 69 mg (25%). R_f = 0.48

DOI: 10.1021/acsomega.6b00060
ACS Omega 2016, 1, 318−333

(9:1 $CHCl_3$/MeOH). Mp: 100 °C. ^{1}H NMR (500 MHz, MeOH-d_4, 298 K, TMS): δ = 8.16 (d, J = 9.5 Hz, 1H, *Acr*), 7.75−7.74 (m, 2H, *Acr*), 7.43−7.426 (m, 1H, *Acr*), 7.34−7.32 (m, 1H, *Acr*), 7.20−7.18 (m, 1H, *Acr*), 3.87 (s, 3H, $-OCH_3$), 3.73 (m, 2H, $-HNCH_2-$), 1.69 (m, 2H, $-CH_2CH_2CH_2-$), 1.32 (m, 2H, $-CH_2CH_2CH_3$), 0.84 (t, J = 7 Hz, 3H, $-CH_2CH_3$). ^{13}C NMR (125 MHz, MeOH-d_4, 298 K, TMS): δ = 155.83, 151.82, 147.58, 135.23, 128.57, 125.78, 125.21, 124.79, 122.73, 116.82, 114.14, 99.79, 54.75, 49.39, 32.90, 19.70, 12.74. MS (MALDI-TOF matrix: α-cyano-4-hydroxycinnamic acid): calculated for $C_{18}H_{19}ClN_2O$ (m/z) 314.12, found 314.93. FTIR (KBr pellet): ν (cm^{-1}) = 3625, 3347, 2962, 2930, 1631, 1568, 1524. Anal. Calcd for $C_{18}H_{19}ClN_2O$: C, 68.67; H, 6.08; N, 8.90. Found: C, 68.53; H, 6.13; N, 8.82.

Synthesis of 6. 6,9-Dichloro-2-methoxy acridine (0.500 g, 1.8 mmol) was dissolved in 1.5 g of phenol at 70 °C by stirring in a 100 mL round-bottom flask under a N_2 atmosphere. Ammonium carbonate (0.35 g, 3.6 mmol) was added to this solution. The reaction mixture was heated to 120 °C and stirred for 2 h and then poured into a 10% NaOH solution. The yellow solid was filtered and washed with 10% NaOH and water and dried under vacuum. Yield: 325 mg (69.71%). Mp: 275 °C. MS (MALDI-TOF matrix: α-cyano-4-hydroxycinnamic acid): calculated for $C_{14}H_{11}ClN_2O$ (m/z) 258.70, found 258.76. Anal. Calcd for $C_{14}H_{11}ClN_2O$: C, 65.00; H, 4.29; N, 10.83. Found: C, 65.17; H, 4.39; N, 10.76.

Synthesis of 7. A mixture of 6,9-dichloro-2-methoxy acridine (1.20 g, 4.30 mmol) and ethylenediamine (20 mL) was heated on a magnetic stirrer at 70 °C for 3 h and then cooled to RT. The addition of ice-cold water into the reaction mixture yielded a yellow precipitate. The yellow precipitate was filtered and dried under vacuum. Yield: 1.00 g (78%). R_f = 0.3 (7:3 $CHCl_3$/MeOH). Mp: 320 °C (decomposed). MS (MALDI-TOF matrix: α-cyano-4-hydroxycinnamic acid): calculated for $C_{16}H_{16}ClN_3O$ (m/z) 301.77, found 301.84. Anal. Calcd for $C_{16}H_{16}ClN_3O$: C, 63.68; H, 5.34; N, 13.92. Found: C, 63.54; H, 5.46; N, 13.83.

In Vitro Parasite Culture. *P. falciparum* strain 3D7 (CQ-sensitive) and W2 (CQ-resistant) (asexual stages) were cultured in human erythrocytes (O^+). The infected erythrocytes were maintained in a RPMI 1640 medium supplemented with 0.2% $NaHCO_3$, 0.5% Albumax-II (lipid-rich bovine serum albumin), gentamycin sulfate (10 μg/mL), and hypoxanthine (27 mg/L) under a gas mixture of 90% N_2, 5% CO_2, and 5% O_2 at 37 °C. These parasites were used for in vitro antimalarial activity assay.

Drug Treatment of the In Vitro Cultured Parasites. The details of stock solutions of all of the drugs and their highest tested concentration are noted in Table S2. All of the DMSO stock solutions were stored at RT and used within 15 days. CQ stock solutions was stored at 4 °C and used within 15 days. For the assay, stock compounds were further diluted in serum-free culture media, and then, serial 2-fold dilutions of each compound were made using complete media in a 24 well plate from their respective highest tested concentration X (mentioned in Table S2) to give respective Y no. of concentrations (mentioned in Table S2) that would be tested. The final DMSO concentration in the wells with the highest drug concentration was not more that 1%, which had no measurable effect on the parasite viability (data not shown). An aliquot of the synchronized ring-stage (8−12 h p.i) culture (*Pf* 3D7 or *Pf* W2) was added to each well of the plates preloaded with serial dilution of drugs to achieve 1% parasitemia and 4% hematocrit. The final culture volume was 1 mL in each well. Each plate had a vehicle (DMSO), positive control drug CQ, and only uninfected RBCs. The plates were kept in a closed chamber under a gas mixture of 5% O_2, 5% CO_2, and 90% N_2, and the chamber was incubated at 37 °C for ∼72 h. After completion of the incubation time (drug exposure), the plates were stored at −80 °C. All tests were conducted in duplicate, and the experiments were reproduced twice.

SYBR Green I Assay for IC_{50} Determination. In vitro antimalarial activity (IC_{50}) was assessed using SYBR Green I assay, an adaptation of the protocols reported elsewhere.[61] The *Plasmodium* cultured plates (24 well) were taken out from −80 °C and thawed completely at RT, and then, each sample was mixed by pipetting. Then, a total volume of 100 μL of lysed culture from each sample was transferred to a new flat-bottom 96 well plate. SYBR Green I in lysis buffer (100 μL) (0.2 μL SYBR Green I/mL lysis buffer; composition of lysis buffer: Tris 200 mM (pH 7.5), EDTA (5 mM), saponin (0.008% w/v), and Triton X-100 (0.08% w/v)) was added to each well. The plates were incubated in the dark at RT for ∼2 h, and fluorescence counts from each well were measured from the bottom of the plate using a Thermo Varioskan plate reader at excitation and emission wave lengths of 485 and 535 nm, respectively. The background reading for an empty well was subtracted using accompanying Varioskan software to afford fluorescence counts for analysis. The IC_{50} values were determined using GraphPad Prism 6 software by fitting the fluorescence counts from all of the test samples in a nonlinear dose−response curve fitting analysis.

Stage-Specific Effects of Compounds and Morphological Analysis. Specific stages of the synchronized culture (ring, trophozoite, and schizont) were treated with compounds for 12 h and then washed to remove the drug followed by resuspension in complete media to complete one life cycle. In parallel, a 36 h (whole cycle) treatment of compounds was given to synchronized ring-stage parasites (∼12 h). The growth of the parasites in each sample (after completion of one cycle) was measured by fluorescence-based SYBR Green I assay. The growth of the triplicate sample with SEM of each stage was plotted against the different concentration of compounds to yield a stage-specific inhibition profile of compounds.

For morphological analysis of antimalarial action or monitoring the growth of hemozoin, samples were taken out from the synchronized ring (∼8−12 h p.i) treated with drugs and untreated culture at different time intervals, and Giemsa-stained parasite pictures were captured using a Nikon light microscope.

Information for the Single Crystal of 1b. CCDC 963831 (**1b**) contains the supplementary crystallographic data for this paper. These data can be obtained free of charge from The Cambridge Crystallographic Data Centre via www.ccdc.cam.ac.uk/data_request/cif. Crystal data for **1b**: $C_{31}H_{22}N_4O_4$, M = 514.52, monoclinic, $C2/c$, a = 25.962 (2) Å, b = 8.9065(8) Å, c = 25.795 (2) Å, α = 90°, β = 110.389(2)°, γ = 90°, V = 5591.0(9) Å^3, Z = 8, Mo Kα radiation (λ = 0.71073 Å), T = 100.0(2) K, μ = 0.083 mm^{-1}, $F(000)$ = 2144, crystal size 0.19 × 0.15 × 0.03 mm^3, Bruker APEX-II CMOS diffractometer, 48 923 reflections, 6948 independent reflections, and 4608 observed reflections [$I > 2\backslash s(I)$ $2\sigma(I)$]; 392 refined parameters, R = 0.0702 and wR_2 = 0.1866.

DOI: 10.1021/acsomega.6b00060
ACS Omega 2016, 1, 318−333

■ ASSOCIATED CONTENT

Supporting Information

The Supporting Information is available free of charge on the ACS Publications website at DOI: 10.1021/acsomega.6b00060.

Analytical characterization of the molecules by NMR and MALDI-TOF MS, crystal data of **1b**, theoretical calculations, UV−vis spectroscopic data, experimental details of cytotoxicity, mitochondrial membrane potential measurements, DNA binding, heme binding, and X-ray crystallography (PDF)

■ AUTHOR INFORMATION

Corresponding Authors

*E-mail: m_pritam@mail.jnu.ac.in (P.M.).
*E-mail: skdhar@mail.jnu.ac.in (S.K.D.).

Notes

The authors declare no competing financial interest.

■ ACKNOWLEDGMENTS

S.K.D., P.M., and N.M. thank the DBT-BUILDER (BT/PR5006/INF/15-3/2012) project in Chemical Biology funded by the Department of Biotechnology (DBT), Govt. of India, and DST-PURSE Projects funded by the Department of Science and Technology, Govt. of India, for financial assistance. S.K.D., P.M., and N.M. acknowledge UPEII, JNU funding for financial assistance. P.M. thanks DST, Govt. of India, for the SwarnaJayanti Fellowship (DST/SJF-02/CSA-02/2013-14). Funding from DST-FIST for the X-ray instrumentation facility and other facilities is highly acknowledged. S.K.D. acknowledges ICMR-CAR core funding and CoE in Molecular Parasitology funded by DBT, India. S.D. thanks CSIR and DBT-BUILDER for research fellowships. S.K.K. and J.S. thanks CSIR and UGC, respectively, for their research fellowship. We thank AIRF (JNU, New Delhi) for the instrumentation facilities.

■ ABBREVIATIONS

NDI, naphthalenediimide; Ac, acridine; SAR, structure−activity relationship; CV, cyclic voltammetry; DPV, differential pulse voltammetry; DMF, *N*,*N*-dimethylformamide; DMSO, dimethyl sulfoxide; Et_3N, triethylamine; h, hour; RT, room temperature; TLC, thin layer chromatography; TE, trisethelenediaminetetraacetic acid

■ REFERENCES

(1) *World Malaria Report*; World Health Organization: UK, 2014.
(2) Richie, T. L.; Saul, A. Progress and challenges for malaria vaccines. *Nature* **2002**, *415*, 694−701.
(3) Seder, R. A.; Chang, L.-J.; Enama, M. E.; Zephir, K. L.; Sarwar, U. N.; Gordon, I. J.; Holman, L. A.; James, E. R.; Billingsley, P. F.; Gunasekera, A.; Richman, A.; Chakravarty, S.; Manoj, A.; Velmurugan, S.; Li, M.; Ruben, A. J.; Li, T.; Eappen, A. G.; Stafford, R. E.; Plummer, S. H.; Hendel, C. S.; Novik, L.; Costner, P. J. M.; Mendoza, F. H.; Saunders, J. G.; Nason, M. C.; Richardson, J. H.; Murphy, J.; Davidson, S. A.; Richie, T. L.; Sedegah, M.; Sutamihardja, A.; Fahle, G. A.; Lyke, K. E.; Laurens, M. B.; Roederer, M.; Tewari, K.; Epstein, J. E.; Sim, B. K. L.; Ledgerwood, J. E.; Graham, B. S.; Hoffman, S. L.; et al. Protection against malaria by intravenous immunization with a nonreplicating sporozoite vaccine. *Science* **2013**, *341*, 1359−1365.
(4) Bray, P. G.; Martin, R. E.; Tilley, L.; Ward, S. A.; Kirk, K.; Fidock, D. A. Defining the role of *Pf* CRT in *Plasmodium falciparum* chloroquine resistance. *Mol. Microbiol.* **2005**, *56*, 323−333.
(5) Dondorp, A. M.; Nosten, F.; Yi, P.; Das, D.; Phyo, A. P.; Tarning, J.; Lwin, K. M.; Ariey, F.; Hanpithakpong, W.; Lee, S. J.; Ringwald, P.; Silamut, K.; Imwong, M.; Chotivanich, K.; Lim, P.; Herdman, T.; An, S. S.; Yeung, S.; Singhasivanon, P.; Day, N. P. J.; Lindegardh, N.; Socheat, D.; White, N. J. Artemisinin resistance in *Plasmodium falciparum* malaria. *N. Engl. J. Med.* **2009**, *361*, 455−467.
(6) Lanfranchi, D. A.; Belorgey, D.; Müller, T.; Vezin, H.; Lanzer, M.; Davioud-Charvet, E. Exploring the trifluoromenadione core as a template to design antimalarial redox-active agents interacting with glutathione reductase. *Org. Biomol. Chem.* **2012**, *10*, 4795−4806.
(7) Meunier, B. Hybrid molecules with a dual mode of action: dream or reality? *Acc. Chem. Res.* **2008**, *41*, 69−77.
(8) Walsh, J.; Bell, A. Hybrid drugs for malaria. *Curr. Pharm. Des.* **2009**, *15*, 2970−2985.
(9) Muregi, F. W.; Ishih, A. Next-generation antimalarial drugs: hybrid molecules as a new strategy in drug design. *Drug Dev. Res.* **2010**, *71*, 20−32.
(10) Huang, P.; Wang, D.; Su, Y.; Huang, W.; Zhou, Y.; Cui, D.; Zhu, X.; Yan, D. Combination of small molecule prodrug and nanodrug delivery: amphiphilic drug−drug conjugate for cancer therapy. *J. Am. Chem. Soc.* **2014**, *136*, 11748−11756.
(11) O'Connell, K. M. G.; Hodgkinson, J. T.; Sore, H. F.; Welch, M.; Salmond, G. P. C.; Spring, D. R. Combating multidrug-resistant bacteria: current strategies for the discovery of novel antibacterials. *Angew. Chem., Int. Ed.* **2013**, *52*, 10706−10733.
(12) Borate, H. B.; Sawargave, S. P.; Chavan, S. P.; Chandavarkar, M. A.; Iyer, R.; Tawte, A.; Rao, D.; Deore, J. V.; Kudale, A. S.; Mahajan, P. S.; Kangire, G. S. Novel hybrids of fluconazole and furanones: design, synthesis and antifungal activity. *Bioorg. Med. Chem. Lett.* **2011**, *21*, 4873−4878.
(13) Godinho, J. L. P.; Georgikopoulou, K.; Calogeropoulou, T.; de Souza, W.; Rodrigues, J. C. F. A novel alkyl phosphocholine-dinitroaniline hybrid molecule exhibits biological activity in vitro against *Leishmania amazonensis*. *Exp. Parasitol* **2013**, *135*, 153−165.
(14) Qiao, Z.; Wang, Q.; Zhang, F.; Wang, Z.; Bowling, T.; Nare, B.; Jacobs, R. T.; Zhang, J.; Ding, D.; Liu, Y.; Zhou, H. Chalcone−benzoxaborole hybrid molecules as potent antitrypanosomal agents. *J. Med. Chem.* **2012**, *55*, 3553−3557.
(15) Coslédan, F.; Fraisse, L.; Pellet, A.; Guillou, F.; Mordmuller, B.; Kremsner, P. G.; Moreno, A.; Mazier, D.; Maffrand, J.-P.; Meunier, B. Selection of a trioxaquine as an antimalarial drug candidate. *Proc. Natl. Acad. Sci. U.S.A.* **2008**, *105*, 17579−17584.
(16) Domarle, O.; Blampain, G.; Agnaniet, H.; Nzadiyabi, T.; Lebibi, J.; Brocard, J.; Maciejewski, L.; Biot, C.; Georges, A. J.; Millet, P. In vitro antimalarial activity of a new organometallic analog, ferrocene-chloroquine. *Antimicrob. Agents Chemother.* **1998**, *42*, 540−544.
(17) Wainwright, M. Acridine-a neglected antibacterial chromophore. *J. Antimicrob. Chemother.* **2001**, *47*, 1−13.
(18) Su, T.-L.; Lin, Y.-W.; Chou, T.-C.; Zhang, X.; Bacherikov, V. A.; Chen, C.-H.; Liu, L. F.; Tsai, T.-J. Potent antitumor 9-anilinoacridines and acridines bearing an alkylating *N*-mustard residue on the acridine chromophore: synthesis and biological activity. *J. Med. Chem.* **2006**, *49*, 3710−3718.
(19) May, B. C. H.; Witkop, J.; Sherrill, J.; Anderson, M. O.; Madrid, P. B.; Zorn, J. A.; Prusiner, S. B.; Cohen, F. E.; Guy, R. K. Structure−activity relationship study of 9-aminoacridine compounds in scrapie-infected neuroblastoma cells. *Bioorg. Med. Chem. Lett.* **2006**, *16*, 4913−4916.
(20) Fang, L.; Appenroth, D.; Decker, M.; Kiehntopf, M.; Roegler, C.; Deuful, T.; Fleck, C.; Peng, S.; Zhang, Y.; Lehmann, J. Synthesis and biological evaluation of NO-donor-tacrine hybrids as hepatoprotective anti-Alzheimer drug candidates. *J. Med. Chem.* **2008**, *51*, 713−716.
(21) Gamage, S. A.; Figgitt, D. P.; Wojcik, S. J.; Ralph, R. K.; Ransijn, A.; Mauel, J.; Yardley, V.; Snowdon, D.; Croft, S. L.; Denny, W. A. Structure−activity relationships for the antileishmanial and antitrypanosomal activities of 1′-substituted 9-anilinoacridines. *J. Med. Chem.* **1997**, *40*, 2634−2642.

DOI: 10.1021/acsomega.6b00060
ACS Omega 2016, 1, 318−333

(22) Yu, X.-M.; Ramiandrasoa, F.; Guetzoyan, L.; Pradines, B.; Quintino, E.; Gadelle, D.; Forterre, P.; Cresteil, T.; Mahy, J.-P.; Pethe, S. Synthesis and biological evaluation of acridine derivatives as antimalarial agents. *ChemMedChem* **2012**, *7*, 587−605.
(23) Gomes, A.; Pérez, B.; Albuquerque, I.; Machado, M.; Prudêncio, M.; Nogueira, F.; Teixeira, C.; Gomes, P. *N*-Cinnamoylation of antimalarial classics: Quinacrine analogues with decreased toxicity and dual-stage activity. *ChemMedChem* **2014**, *9*, 305−310.
(24) Dana, S.; Prusty, D.; Dhayal, D.; Gupta, M. K.; Dar, A.; Sen, S.; Mukhopadhyay, P.; Adak, T.; Dhar, S. K. Potent antimalarial activity of acriflavine in vitro and in vivo. *ACS Chem. Biol.* **2014**, *9*, 2366−2373.
(25) Pal, C.; Bandyopadhyay, U. Redox-active antiparasitic drugs. *Antioxid. Redox Signaling* **2012**, *17*, 555−582.
(26) Krauth-Siegel, R. L.; Bauer, H.; Schirmer, R. H. Dithiol proteins as guardians of the intracellular redox milieu in parasites: old and new drug targets in trypanosomes and malaria-causing plasmodia. *Angew. Chem., Int. Ed.* **2005**, *44*, 690−715.
(27) Müller, T.; Johann, L.; Jannack, B.; Brückner, M.; Lanfranchi, D. A.; Bauer, H.; Sanchez, C.; Yardley, V.; Deregnaucourt, C.; Schrével, J.; Lanzer, M.; Schirmer, R. H.; Davioud-Charvet, E. Glutathione reductase-catalyzed cascade of redox reactions to bioactivate potent antimalarial 1,4- naphthoquinones−a new strategy to combat malarial parasites. *J. Am. Chem. Soc.* **2011**, *133*, 11557−11571.
(28) Vaidya, A. B.; Mather, M. W. Mitochondrial evolution and functions in malaria parasites. *Annu. Rev. Microbiol.* **2009**, *63*, 249−267.
(29) Ehrhardt, K.; Davioud-Charvet, E.; Ke, H.; Vaidya, A. B.; Lanzer, M.; Deponte, M. The antimalarial activities of methylene blue and the 1,4-naphthoquinone 3-[4-(trifluoromethyl)benzyl]-menadione are not due to inhibition of the mitochondrial electron transport chain. *Antimicrob. Agents Chemother.* **2013**, *57*, 2114−2120.
(30) Suraru, S.-L.; Würthner, F. Strategies for the synthesis of functional Naphthalenediimides. *Angew. Chem., Int. Ed.* **2014**, *53*, 7428−7448.
(31) Sakai, N.; Mareda, J.; Vauthey, E.; Matile, S. Core-substituted naphthalenediimides. *Chem. Commun.* **2010**, *46*, 4225−4237.
(32) He, T.; Stolte, M.; Burschka, C.; Hansen, N. H.; Musiol, T.; Kälblein, D.; Pflaum, J.; Tao, X.; Brill, J.; Würthner, F. Single-crystal field-effect transistors of new Cl_2-NDI polymorph processed by sublimation in air. *Nat. Commun.* **2015**, *6*, 5954.
(33) Zhao, Y.; Cotelle, Y.; Avestro, A.-J.; Sakai, N.; Matile, S. Asymmetric anion-π catalysis: Enamine addition to nitroolefins on π-acidic surfaces. *J. Am. Chem. Soc.* **2015**, *137*, 11582−11585.
(34) Cotelle, Y.; Benz, S.; Avestro, A.-J.; Ward, T. R.; Sakai, N.; Matile, S. Anion-π catalysis of enolate chemistry: Rigidified leonard turns as a general motif to run reactions on aromatic surfaces. *Angew. Chem., Int. Ed.* **2016**, *55*, 4275−4279.
(35) Takai, A.; Yasuda, T.; Ishizuka, T.; Kojima, T.; Takeuchi, M. A directly linked ferrocene−naphthalenediimide conjugate: precise control of stacking structures of π-systems by redox stimuli. *Angew. Chem., Int. Ed.* **2013**, *52*, 9167−9171.
(36) Takai, A.; Sakamaki, D.; Seki, S.; Matsushita, Y.; Takeuchi, M. Ferrocene-substituted naphthalenediimide with broad absorption and electron-transport properties in the segregated-stack structure. *Chem.−Eur. J.* **2016**, *22*, 7385−7388.
(37) Kulkarni, C.; George, S. J. Carbonate linkage bearing naphthalenediimides: selfassembly and photophysical properties. *Chem.−Eur. J* **2014**, *20*, 4537−4541.
(38) Poddutoori, P. K.; Zarrabi, N.; Moiseev, A. G.; Gumbau-Brisa, R.; Vassiliev, S.; van der Est, A. Long-lived charge separation in novel axial donor−porphyrin−acceptor triads based on tetrathiafulvalene, aluminum(III) porphyrin and naphthalenediimide. *Chem.−Eur. J* **2013**, *19*, 3148−3161.
(39) Lu, X.; Zhu, W.; Xie, Y.; Li, X.; Gao, Y.; Li, F.; Tian, H. Near-IR core-substituted naphthalenediimide fluorescent chemosensors for zinc ions: ligand effects on PET and ICT channels. *Chem.−Eur. J.* **2010**, *16*, 8355−8364.
(40) Manchineella, S.; Prathyusha, V.; Priyakumar, U. D.; Govindaraju, T. Solvent-induced helical assembly and reversible chiroptical switching of chiral cyclic-dipeptide-functionalized naphthalenediimides. *Chem.−Eur. J.* **2013**, *19*, 16615−16624.
(41) Liu, Z.-R.; Hecker, K. H.; Rill, R. L. Selective DNA binding of (*N*-alkylamine)-substituted naphthalene imides and diimides to G + C-rich DNA. *J. Biomol. Struct. Dyn.* **1996**, *14*, 331−339.
(42) Tumiatti, V.; Milelli, A.; Minarini, A.; Micco, M.; Campani, A. G.; Roncuzzi, L.; Baiocchi, D.; Marinello, J.; Capranico, G.; Zini, M.; Stefanelli, C.; Melchiorre, C. Design, synthesis, and biological evaluation of substituted naphthalene imides and diimides as anticancer agent. *J. Med. Chem.* **2009**, *52*, 7873−7877.
(43) Wang, Y.; Zhang, X.; Zhao, J.; Xie, S.; Wang, C. Non-hematotoxic naphthalene diimide modified by polyamine: synthesis and biological evaluation. *J. Med. Chem.* **2012**, *55*, 3502−3512.
(44) Ohnmacht, S. A.; Marchetti, C.; Gunaratnam, M.; Besser, R. J.; Haider, S. M.; Vita, G. D.; Lowe, H. L.; Mellinas-Gomez, M.; Diocou, S.; Robson, M.; Šponer, J.; Islam, B.; Pedley, R. B.; Hartley, J. A.; Neidle, S. A G-quadruplex-binding compound showing anti-tumour activity in an in vivo model for pancreatic cancer. *Sci. Rep.* **2015**, *5*, 11385.
(45) Hampel, S. M.; Pepe, A.; Greulich-Bode, K. M.; Malhotra, S. V.; Reszka, A. P.; Veith, S.; Boukamp, P.; Neidle, S. Mechanism of the antiproliferative activity of some naphthalene diimide G-quadruplex ligands. *Mol. Pharmacol.* **2013**, *83*, 470−478.
(46) McKnight, R. E.; Reisenauer, E.; Pintado, M. V.; Polasani, S. R.; Dixon, D. W. Substituent effect on the preferred DNA binding mode and affinity of a homologous series of naphthalene diimides. *Bioorg. Med. Chem. Lett.* **2011**, *21*, 4288−4291.
(47) Avinash, M. B.; Govindaraju, T. Amino Acid Derivatized Arylenediimides: A Versatile Modular Approach for Functional Molecular Materials. *Adv. Mater.* **2012**, *24*, 3905−3922.
(48) Chu, Y.; Hoffman, D. W.; Iverson, B. L. A pseudocatenane structure formed between DNA and a cyclic bisintercalator. *J. Am. Chem. Soc.* **2009**, *131*, 3499−3508.
(49) Holman, G. G.; Zewail-Foote, M.; Smith, A. R.; Johnson, K. A.; Iverson, B. L. A sequence-specific threading tetra-intercalator with an extremely slow dissociation rate constant. *Nat. Chem.* **2011**, *3*, 875−881.
(50) Wu, Y.; Nalluri, S. K. M.; Young, R. M.; Krzyaniak, M. D.; Margulies, E. A.; Stoddart, J. F.; Wasielewski, M. R. Charge and spin transport in an organic molecular square. *Angew. Chem., Int. Ed.* **2015**, *54*, 11971−11977.
(51) Bruns, C. J.; Li, J.; Frasconi, M.; Schneebeli, S. T.; Iehl, J.; de Rouville, H.-P. J.; Stupp, S. I.; Voth, G. A.; Stoddart, J. F. An electrochemically and thermally switchable donor−acceptor [c2]daisy chain rotaxane. *Angew. Chem., Int. Ed.* **2014**, *53*, 1953−1958.
(52) Ajayakumar, M. R.; Mukhopadhyay, P. Naphthalene-bis-hydrazimide: radical anions and ICT as new bimodal probes for differential sensing of a library of amines. *Chem. Commun.* **2009**, 3702−3704.
(53) Ajayakumar, M. R.; Mukhopadhyay, P.; Yadav, S.; Ghosh, S. Single-electron transfer driven cyanide sensing: a new multimodal approach. *Org. Lett.* **2010**, *12*, 2646−2649.
(54) Kumar, S.; Ajayakumar, M. R.; Hundal, G.; Mukhopadhyay, P. Extraordinary stability of NDI radical ion and its ultra-electron-deficient precursor: strategic role of the phosphonium group. *J. Am. Chem. Soc.* **2014**, *136*, 12004−12010.
(55) Brochsztain, S.; Rodrigues, M. A.; Demets, G. J. F.; Politi, M. J. Stabilization of naphthalene-1,8,4,5-dicarboximide radicals in zirconium phosphonate solid materials and thin films. *J. Mater. Chem.* **2002**, *12*, 1250−1255.
(56) Ashkenasy, N.; Horne, W. S.; Ghadiri, M. R. Design of self-assembling peptide nanotubes with delocalized electronic states. *Small* **2006**, *2*, 99−102.
(57) Zheng, J.; Qiao, W.; Wan, X.; Gao, J. P.; Wang, Z. Y. Near-Infrared electrochromic and chiroptical switching materials: Design, synthesis, and characterization of chiral organogels containing stacked naphthalenediimide chromophores. *Chem. Mater.* **2008**, *20*, 6163−6168.

DOI: 10.1021/acsomega.6b00060
ACS Omega 2016, 1, 318−333

(58) Guetzoyan, L.; Yu, X.-M.; Ramiandrasoa, F.; Pethe, S.; Rogier, C.; Pradines, B.; Cresteil, T.; Perrée-Fauvet, M.; Mahy, J.-P. Antimalarial Acridines: synthesis, in vitro activity against *P. falciparum* and interaction with hematin. *Bioorg. Med. Chem.* **2009**, *17*, 8032−8039.
(59) Ishikawa, Y.; Yamashita, A.; Uno, T. Efficient photo cleavage of DNA by cationic porphyrin−acridine hybrids with the effective length of diamino linkage. *Chem. Pharm. Bull.* **2001**, *49*, 287−293.
(60) Bonse, S.; Santelli-Rouvier, C.; Barbe, J.; Krauth-Siegel, R. L. Inhibition of *Trypanosoma cruzi* trypanothione reductase by acridines: kinetic studies and structure−activity relationships. *J. Med. Chem.* **1999**, *42*, 5448−5454.
(61) Smilkstein, M.; Sriwilaijaroen, N.; Kelly, J. X.; Wilairat, P.; Riscoe, M. Simple and inexpensive fluorescence-based technique for high-throughput antimalarial drug screening. *Antimicrob. Agents Chemother.* **2004**, *48*, 1803−1806.
(62) Guetzoyan, L.; Ramiandrasoa, F.; Dorizon, H.; Desprez, C.; Bridoux, A.; Rogier, C.; Pradines, B.; Perrée-Fauvet, M. In vitro efficiency of new acridyl derivatives against *Plasmodium falciparum*. *Bioorg. Med. Chem.* **2007**, *15*, 3278−3289.
(63) Foley, M.; Tilley, L. Quinoline antimalarials: mechanisms of action and resistance and prospects for new agents. *Pharmacol. Ther.* **1998**, *79*, 55−87.
(64) Egan, T. J.; Ncokazi, K. K. Quinoline antimalarials decrease the rate of β-hematin formation. *J. Inorg. Biochem.* **2005**, *99*, 1532−1539.
(65) Kumar, S.; Guha, M.; Choubey, V.; Maity, P.; Bandyopadhyay, U. Antimalarial drugs inhibiting hemozoin (β-hematin) formation: a mechanistic update. *Life Sci.* **2007**, *80*, 813−828.
(66) Buller, R.; Peterson, M. L.; Almarsson, O.; Leiserowitz, L. Quinoline binding site on malarial pigment crystal: A rational pathway for antimalarial design. *Cryst. Growth Des.* **2002**, *2*, 553−562.
(67) Valdés, A. F.-C. Acridine and acridinones: old and new structures with antimalarial activity. *Open Med. Chem. J.* **2011**, *5*, 11−20.
(68) Auparakkitanon, S.; Noonpakdee, W.; Ralph, R. K.; Denny, W. A.; Wilairat, P. Antimalarial 9-anilinoacridine compounds directed at hematin. *Antimicrob. Agents Chemother.* **2003**, *47*, 3708−3712.
(69) Egan, T. J.; Hunter, R.; Kaschula, C. H.; Marques, H. M.; Misplon, A.; Walden, J. Structure-function relationships in amino-quinolines: effect of amino and chloro groups on quinoline−hematin complex formation, inhibition of β-hematin formation, and anti-plasmodial activity. *J. Med. Chem.* **2000**, *43*, 283−291.
(70) Lavrado, J.; Cabal, G. G.; Prudêncio, M.; Mota, M. M.; Gut, J.; Rosenthal, P. J.; Díaz, C.; Guedes, R. C.; dos Santos, D. J. V. A.; Bichenkova, E.; Douglas, K. T.; Moreira, R.; Paulo, A. Incorporation of basic side chains into cryptolepine scaffold: structure-antimalarial activity relationships and mechanistic studies. *J. Med. Chem.* **2011**, *54*, 734−750.
(71) Natarajan, J. K.; Alumasa, J. N.; Yearick, K.; Ekoue-Kovi, K. A.; Casabianca, L. B.; de Dios, A. C.; Wolf, C.; Roepe, P. D. 4-*N*-, 4-*S*-, and 4-*O*-chloroquine analogues: influence of side chain length and quinolyl nitrogen pK_a on activity vs chloroquine resistant malaria. *J. Med. Chem.* **2008**, *51*, 3466−3479.
(72) de Villiers, K. A.; Gildenhuys, J.; le Roex, T. Iron(III) protoporphyrin IX complexes of the antimalarial Cinchona alkaloids quinine and quinidine. *ACS Chem. Biol.* **2012**, *7*, 666−671.
(73) Gorka, A. P.; de Dios, A.; Roepe, P. D. Quinoline drug−heme interactions and implications for antimalarial cytostatic versus cytocidal activities. *J. Med. Chem.* **2013**, *56*, 5231−5246.
(74) Weissbuch, I.; Leiserowitz, L. Interplay between malaria, crystalline hemozoin formation, and antimalarial drug action and design. *Chem. Rev.* **2008**, *108*, 4899−4914.
(75) Madrid, P. B.; Liou, A. P.; DeRisi, J. L.; Guy, R. K. Incorporation of an intramolecular hydrogen-bonding motif in the side chain of 4-aminoquinolines enhances activity against drug-resistant P. falciparum. *J. Med. Chem.* **2006**, *49*, 4535−4543.
(76) Avdeef, A. Physicochemical profiling (solubility, permeability and charge state). *Curr. Top. Med. Chem.* **2001**, *1*, 277−351.
(77) Caron, G.; Reymond, F.; Carrupt, P.-A.; Girault, H. H.; Testa, B. Combined molecular lipophilicity descriptors and their role in understanding intramolecular effects. *Pharm. Sci. Technol. Today* **1999**, *2*, 327−335.
(78) Lipinski, C. A.; Lombardo, F.; Dominy, B. W.; Feeney, P. J. Experimental and computational approaches to estimate solubility and permeability in drug discovery and development settings. *Adv. Drug Delivery Rev.* **2001**, *46*, 3−26.
(79) Lipinski, C. A.; Lombardo, F.; Dominy, B. W.; Feeney, P. J. Experimental and computational approaches to estimate solubility and permeability in drug discovery and development settings. *Adv. Drug Delivery Rev.* **1997**, *23*, 3−25.
(80) ChemAxon Home page. http://www.chemaxon.com (Mar 8, 2015).
(81) Ehsanian, R.; Van Waes, C.; Feller, S. M. Beyond DNA binding—a review of the potential mechanisms mediating quinacrine's therapeutic activities in parasitic infections, inflammation, and cancers. *Cell Commun. Signaling* **2011**, *9*, 13−30.
(82) Pandey, A. V.; Babbarwal, V. K.; Okoyeh, J. N.; Joshi, R. M.; Puri, S. K.; Singh, R. L.; Chauhan, V. S. Hemozoin formation in malaria: a two-step process involving histidine-rich proteins and lipids. *Biochem. Biophys. Res. Commun.* **2003**, *308*, 736−743.
(83) Francis, S. E.; Sullivan, D. J., Jr.; Goldberg, D. E. Hemoglobin metabolism in the malaria parasite *Plasmodium falciparum*. *Annu. Rev. Microbiol.* **1997**, *51*, 97−123.
(84) Egan, T. J.; Mavuso, W. W.; Ross, D. C.; Marques, H. M. Thermodynamic factors controlling the interaction of quinoline antimalarial drugs with ferriprotoporphyrin IX. *J. Inorg. Biochem.* **1997**, *68*, 137−145.
(85) Singh, K.; Kaur, H.; Smith, P.; de Kock, C.; Chibale, K.; Balzarini, J. Quinoline−pyrimidine hybrids: synthesis, antiplasmodial activity, SAR, and mode of action studies. *J. Med. Chem.* **2014**, *57*, 435−448.
(86) Narayanaswamy, N.; Das, S.; Samanta, P. K.; Banu, K.; Sharma, G. P.; Mondal, N.; Dhar, S. K.; Pati, S. K.; Govindaraju, T. Sequence-specific recognition of DNA minor groove by an NIR-fluorescence switch-on probe and its potential applications. *Nucleic Acids Res.* **2015**, *43*, 8651−8663.
(87) Narayanaswamy, N.; Kumar, M.; Das, S.; Sharma, R.; Samanta, P. K.; Pati, S. K.; Dhar, S. K.; Kundu, T. K.; Govindaraju, T. A thiazole coumarin (TC) turn-on fluorescence probe for AT-base pair detection and multipurpose applications in different biological systems. *Sci. Rep* **2014**, *4*, 6476−6485.
(88) Kabil, O.; Banerjee, R. Redox biochemistry of hydrogen sulfide. *J. Biol. Chem.* **2010**, *285*, 21903−21907.

DOI: 10.1021/acsomega.6b00060
ACS Omega 2016, 1, 318−333